

Effective multi-body $SU(N)$ -symmetric interactions of ultracold fermionic atoms on a 3-D lattice

M A Perlin* and A M Rey

JILA, National Institute of Standards and Technology and University of Colorado,

440 UCB, Boulder, Colorado 80309, USA

Center for Theory of Quantum Matter,

440 UCB, Boulder, Colorado 80309, USA and

Department of Physics, University of Colorado,

390 UCB, Boulder, Colorado 80309, USA

Abstract

Rapid advancements in the experimental capabilities with ultracold alkaline-earth-like atoms (AEAs) bring to a surprisingly near term the prospect of performing quantum simulations of spin models and lattice field theories exhibiting $SU(N)$ symmetry. Motivated in particular by recent experiments preparing high density samples of strongly interacting ^{87}Sr atoms in a three-dimensional optical lattice, we develop a low-energy effective theory of fermionic AEAs which exhibits emergent multi-body $SU(N)$ -symmetric interactions, where N is the number of atomic nuclear spin levels. Our theory is limited to the experimental regime of (i) a deep lattice, with (ii) at most one atom occupying each nuclear spin state on any lattice site. The latter restriction is a consequence of initial ground-state preparation. We fully characterize the low-lying excitations in our effective theory, and compare predictions of many-body interaction energies with direct measurements of many-body excitation spectra in an optical lattice clock. Our work makes the first step in enabling a controlled, bottom-up experimental investigation of multi-body $SU(N)$ physics.

Keywords: *ultracold atoms, optical lattices, $SU(N)$ magnetism, multi-body interactions*

* mika.perlin@gmail.com

CONTENTS

I. Introduction	3
II. Background and overview	5
III. Low-energy effective theory	10
A. Diagrammatic representation of effective Hamiltonians	13
B. Effective two-body interactions and renormalization	15
C. Effective three-body interactions at second order	17
D. Effective three-body interactions at third order	18
E. Effective four-body interactions at third order	21
IV. Low-excitation Hamiltonians, eigenstates, and spectra	23
A. Many-body state spectroscopy	24
B. Experimental signatures and comparison	26
C. Orbital-state dynamics of a nuclear spin mixture	30
V. Summary and outlook	33
Acknowledgements	34
Appendices	34
A. Derivation of the effective Hamiltonian expansion	34
B. Diagram counting and symmetry factors	37
C. Effective coupling constants in a lattice	39
D. Momentum-dependent s -wave interactions	41
E. Bounds on theoretical uncertainties from inter-site effects	42
F. Perturbative parameters for the effective theory	45
G. Low-excitation M -body Hamiltonian coefficients	45

I. INTRODUCTION

Fermionic alkaline-earth atoms (AEAs), in addition to other atoms such as ytterbium (Yb) sharing similar electronic structure, are currently the building blocks of the most precise atomic clocks in the world [1–3]. These atoms have a unique, ultra-narrow optical transition between metastable 1S_0 and 3P_0 electronic orbital states, i.e. the “clock states”, that allows for coherence times which can exceed 100 seconds [4, 5]. Furthermore, AEAs can be trapped in fully controllable optical lattice potentials and interrogated with ultra-stable lasers that can resolve and probe their rich hyperfine spectra, consisting of N different nuclear spin levels with N as large as 10 in strontium (^{87}Sr) and 6 in ytterbium (^{173}Yb).

In 2015 the ^{87}Sr optical lattice clock (OLC) at JILA, operated in a one-dimensional (1-D) lattice at microkelvin temperatures, achieved a total fractional uncertainty of 2×10^{-18} [6, 7]. More recently (2017), a new generation of OLCs became operational at JILA, interrogating a Fermi degenerate gas of ^{87}Sr atoms in a 3-D lattice at nanokelvin temperatures [8]. All of these atoms’ degrees of freedom, including the electronic orbital, nuclear spin, and motional states, can be fully controlled with high fidelity in a 3-D lattice [9–12]. With frequency measurements reaching the 10^{-19} fractional uncertainty level, the new OLCs are thus enabling an exciting opportunity to probe, for the first time, quantum dynamics with sub-millihertz spectral resolution [8].

A wonderful consequence of the efforts to build better clocks is the development of highly controllable quantum simulators of many-body systems in the strongly-interacting regime, where inter-particle interactions set the largest energy scale relevant for system dynamics [8, 13, 14]. The marriage between precision clock spectroscopy and quantum many-body physics [15–20] has an enormous potential to enable novel explorations of physics for the same reason that makes AEAs such remarkable time-keepers. Specifically, due to the lack of electronic orbital angular momentum in the 1S_0 and 3P_0 states, AEAs exhibit decoupled orbital and nuclear spin degrees of freedom. For atoms with N nuclear spin levels, this decoupling leads to nuclear-spin-conserving $\text{SU}(N)$ -symmetric interactions governed entirely by orbital-state parameters [15, 19, 21].

The presence of this exotic $\text{SU}(N)$ symmetry in a highly controllable experimental plat-

form opens the door to experimental studies of e.g. the $SU(N)$ Heisenberg model, whose phase diagram is believed to exhibit features such as a chiral spin liquid (CSL) phase with topological order and fractional statistics [22–24]. In addition to illuminating open questions in our understanding of the fractional quantum Hall effect and unconventional superconductivity [25–27], the CSL can support non-Abelian excitations which allow for universal topological quantum computation [23, 28]. Harnessing the $SU(N)$ -symmetric interactions of AEs might also enable the simulation of various lattice gauge theories [29, 30], some of which share important qualitative features with quantum chromodynamics such as few-body bound states and confinement [31, 32]. These direct, quantum simulations have an extraordinary potential to provide novel insights by circumventing e.g. severe sign problems which plague classical simulations of strongly interacting fermionic systems [29, 33].

In this work, we investigate the first experimental capabilities with ultracold fermionic AEs to prepare high-density samples in a 3-D lattice with multiple occupation of individual lattice sites [34]. Specifically, we consider ground-state preparation of isolated few-body systems in the deep-lattice limit, and carry out a bottom-up investigation of emergent multi-body interactions on multiply-occupied lattice sites. These multi-body interactions appear in a low-energy effective theory of the atoms, and inherit the $SU(N)$ symmetry of their bare, pair-wise interactions, thereby enabling experimental studies of multi-body $SU(N)$ physics through the exquisite capabilities with OLCs. Our theory is limited to the experimental regime of at most one atom occupying each nuclear spin state on any lattice site, which is a consequence of the experimental protocol which starts with all atoms in the ground state.

Though effective multi-body interactions have previously been studied in the context of harmonically [35, 36] and lattice-confined [37] neutral bosons prepared in a single hyperfine state, our work deals for the first time with fermions that have internal degrees of freedom and multiple collisional parameters. Some past work has detected experimental signatures of multi-body interactions in the form of quantum phase revivals [38]. We instead compare the many-body interaction energies predicted by our low-energy effective theory to the experimental measurements of the density-dependent orbital excitation spectra performed in ref. [34], similarly to the measurements with bosons performed in ref. [39]. To facilitate this comparison of excitation spectra and to characterize the low-lying excitations in our effective theory, we consider a restriction of our theory to states with at most one orbital excitation per lattice site. In this case, we find that the $SU(N)$ symmetry of atomic collisions allow

the effective multi-body interactions to take a remarkably simple form.

The remainder of this paper is structured as follows. In section II we summarize the experimental procedures relevant to our work, provide an overview of the one- and two-body physics of ultracold atoms in a deep lattice, and preview our main technical results. In section III we discuss our method for deriving a low-energy effective theory, provide a perturbative expansion for the net effective Hamiltonian, and compute all M -body Hamiltonians through third order in the low-energy effective theory. We then analyze the low-lying excitations of the effective theory in section IV, comparing spectral predictions with experimental measurements, and study the orbital-state dynamics of nuclear spin mixtures interrogated via Rabi spectroscopy. Finally, we summarize and conclude our findings in section V, and provide some discussion of future outlooks.

II. BACKGROUND AND OVERVIEW

The work in this paper is closely tied to the experimental work reported in ref. [34]; we begin with a short summary of the relevant experimental procedures therein. The experiment begins by preparing a degenerate gas of 10^4 - 10^5 (fermionic) ^{87}Sr atoms in a uniform mixture of their ten nuclear spin states and at ~ 0.1 of their fermi temperature (~ 10 nanokelvin) [8, 40]. This gas is loaded into a primitive cubic optical lattice at the “magic wavelength” for which both ground (1S_0) and first-excited (3P_0) electronic orbital states of the atoms experience the same lattice potential [41]. Lattice depths along the principal axes of the lattice are roughly equal in magnitude, with a geometric mean that can be varied from 30 to $80 E_R$, where $E_R \approx 3.5 \times 2\pi$ kHz is the lattice photon recoil energy of the atoms (with the reduced Planck constant $\hbar = 1$ throughout this paper). These lattice depths are sufficiently large as to neglect tunneling on the time scales relevant to the experiment. The temperature of the atoms is also low enough to neglect thermal occupation of motional states outside the ground-state manifold.

Once loaded into an optical lattice, atoms are addressed by an external (“clock”) interrogation laser with an ultranarrow (26 mHz) linewidth, detuned by Δ from the single-atom $^1S_0 - ^3P_0$ transition frequency ω_0 . After a fixed interrogation time, the experiment turns off the interrogation laser, removes all ground-state (1S_0) atoms from the lattice, and uses absorption imaging to count the remaining excited-state (3P_0) atoms. Non-interacting

atoms in singly-occupied lattice sites feature the typical single particle lineshape peaked at $\Delta = 0$. The lineshapes of multiply-occupied lattice sites, meanwhile, are shifted by inter-atomic interactions, which results in spectroscopic peaks (i.e. local maxima in excited-state atom counts) away from $\Delta = 0$. A sweep across different detunings Δ (on the scale of inter-atomic interaction energies) thus constitutes a measurement of the many-body orbital excitation spectrum. We note that this spectroscopic protocol addresses only singly-excited orbital states of lattice sites. Doubly-excited states are off resonant due to (i) the interaction-induced non-linearity (\sim kHz) of the orbital excitation energies, and (ii) the ultranarrow linewidth (\sim mHz) of the interrogation laser.

Although an external trapping potential will generally break discrete translational symmetry of the lattice, any background inhomogeneity can be made negligible by spectroscopically addressing a sufficiently small region of the lattice [34]. Throughout this paper, we work strictly in the deep-lattice regime with negligible tunneling between lattice sites. We also neglect any lattice inhomogeneities and assume that both atomic orbital states (i.e. 1S_0 and 3P_0) experience identical lattice potentials. The single-particle Hamiltonian of the atoms can then be written in the form

$$H_0 = \sum_{i,n,\mu,s} E_n \hat{c}_{in\mu s}^\dagger \hat{c}_{in\mu s}, \quad (1)$$

where $\hat{c}_{in\mu s}$ is a fermionic operator which annihilates a single atom on lattice site $i \in \mathbb{Z}^3$ in motional state $n \in \mathbb{N}_0^3$ with nuclear spin $\mu \in \{-I, -I+1, \dots, I\}$ (i.e. projected onto a quantization axis) and orbital state $s \in \{g, e\}$; and E_n is the energy of a single atom in motional state n . In a harmonic trap approximation we would have $E_n = (3/2 + n_x + n_y + n_z)\omega$ for an on-site angular trap frequency ω , but in general the anharmonicity of the lattice potential will cause a non-negligible shift in motional state energies.

In the absence of hyperfine coupling, as when addressing the spinless 1S_0 (g) and 3P_0 (e) orbital states of AEAs, interactions between any two atoms are governed by their orbital states alone, and are therefore characterized by four scattering lengths a_X with $X \in \{gg, eg^-, eg^+, ee\}$, where the $+$ ($-$) superscript denotes symmetrization (antisymmetrization) of a two-body orbital state under particle exchange. In the low-energy limit, we can write the bare two-body interaction Hamiltonian in the form [42]

$$H_{\text{int}} = \sum_{\substack{\mu < \nu \\ s}} G_s \int d^3x \hat{\rho}_{\mu s} \hat{\rho}_{\nu s} + G_+ \sum_{\mu, \nu} \int d^3x \hat{\rho}_{\mu, e} \hat{\rho}_{\nu, g} + G_- \sum_{\mu, \nu} \int d^3x \hat{\psi}_{\mu, e}^\dagger \hat{\psi}_{\nu, g}^\dagger \hat{\psi}_{\nu, e} \hat{\psi}_{\mu, g}, \quad (2)$$

where $\hat{\psi}_{\mu s}$ is a fermionic field operator for atoms with nuclear spin μ and orbital state s ; $\hat{\rho}_{\mu s} \equiv \hat{\psi}_{\mu s}^\dagger \hat{\psi}_{\mu s}$ is an atomic density field operator; and the coupling constants G_X are defined in terms of the scattering lengths a_Y by

$$G_{s=g,e} \equiv \frac{4\pi}{m_A} a_{ss}, \quad G_{\pm} \equiv \frac{2\pi}{m_A} (a_{eg+} \pm a_{eg-}), \quad (3)$$

where m_A is the mass of a single atom. Defining for brevity

$$G_{st}^{qr} \equiv \begin{cases} G_q & q = r = s = t \\ G_+ & q \neq r \text{ and } (q, r) = (s, t) \\ G_- & q \neq r \text{ and } (q, r) = (t, s) \\ 0 & \text{otherwise} \end{cases}, \quad (4)$$

where $q, r, s, t \in \{g, e\}$ are orbital state indices, we can alternately write the bare two-body interaction Hamiltonian in the more compact form

$$H_{\text{int}} = \frac{1}{2} \sum_{\substack{q,r,s,t \\ \mu,\nu}} G_{st}^{qr} \int d^3x \hat{\psi}_{\mu s}^\dagger \hat{\psi}_{\nu t}^\dagger \hat{\psi}_{\nu r} \hat{\psi}_{\mu q}. \quad (5)$$

For nuclear spins μ, ν , the symbol G_{st}^{qr} gives the coupling constant between the two-atom states $(\mu, q) + (\nu, r) \leftrightarrow (\mu, s) + (\nu, t)$.

Note that the Hamiltonian in (5) is not the true microscopic interaction Hamiltonian of AEAs, but rather a generic form for a low-energy effective field theoretic description of two-body interactions [17, 21, 35–37, 42–44]. There are therefore two important points to keep in mind concerning our use of (5) to describe two-body interactions. First, the use of effective field theory generically gives rise to divergences that must be dealt with either through regularization, e.g. of the zero-range interaction potential implicitly assumed in the expression of (5) [45], or through renormalization of the coupling constants in the theory. We chose the latter approach, as we will in any case find it convenient to renormalize the coupling constants in the effective theory developed in section III. The choice of method to regulate divergences has no effect on the underlying physics.

Second, (5) is only the first term in a low-energy expansion of two-body interactions in effective field theory, which generally includes additional terms containing derivatives of field operators. Derivative terms correspond to the dependence of two-body scattering on the relative momentum k of particles involved, with $k \rightarrow 0$ in the zero-energy limit. In the present case of s -wave scattering, the leading dependence of the two-body interaction

Hamiltonian on the relative momentum k can be captured by use of an energy-dependent pseudo-potential, which amounts to using a k -dependent effective scattering length [46]. This effective scattering length can be determined by expanding the s -wave collisional phase shift in powers of the relative momentum k [45, 47]. Details of this expansion will depend on the characteristic length scale of finite-range interactions. In our work, these corrections to (5) will be relevant only for the calculation of two-body interaction energies, appearing at third order in the coupling constants G_X . As we are primarily interested in M -body interactions for $M \geq 3$, we defer this calculation to Appendix D. We note that our approach of using an unregularized contact potential, renormalizing coupling constants, and separately accounting for momentum-dependent scattering is essentially the same as the approach used for similar calculations in refs. [35–37]. While this approach does not provide insight into the microscopic structure of inter-atomic interactions, it is suitable for the phenomenological description of these interactions, and particular for our eventual development of a low-energy effective theory.

We now expand the field operators $\hat{\psi}_{\mu s}$ in the Wannier basis for a 3-D lattice, such that $\hat{\psi}_{\mu s}(x) = \sum_{i,n} \phi_{in}(x) \hat{c}_{in\mu s}$ with spatial wavefunctions ϕ_{in} and fermionic annihilation operators $\hat{c}_{in\mu s}$ indexed by lattice sites i and motional states n . Invoking the tight-binding approximation, we assume that the spatial overlap integral in (5) is negligible unless all wavefunctions are localized at the same lattice site; we discuss the breakdown of this approximation and its consequences for our low-energy effective theory in Appendix E. The relevant spatial overlap integral is then

$$K_{mn}^{k\ell} \equiv \int d^3x \phi_{im}^* \phi_{in}^* \phi_{i\ell} \phi_{ik}, \quad (6)$$

which for a lattice with discrete translational invariance is independent of the lattice site i . The two-body interaction Hamiltonian can be written in terms of this overlap integral as

$$H_{\text{int}} = \frac{1}{2} \sum_{\substack{i,k,\ell,m,n \\ q,r,s,t \\ \mu,\nu}} K_{mn}^{k\ell} G_{st}^{qr} \hat{c}_{im\mu s}^\dagger \hat{c}_{in\nu t}^\dagger \hat{c}_{i\ell\nu r} \hat{c}_{ik\mu q} \equiv \frac{1}{2} \sum K_{mn}^{k\ell} G_{st}^{qr} \hat{c}_{m\mu s}^\dagger \hat{c}_{n\nu t}^\dagger \hat{c}_{\ell\nu r} \hat{c}_{k\mu q}, \quad (7)$$

where for brevity we will henceforth suppress the identical site index (i) on all operators, and implicitly sum over all free indices in a summand (i.e. indices which do not have a fixed value). We may also at times suppress motional state indices on the overlap integral $K_{mn}^{k\ell}$, in which case the suppressed indices are implicitly zero (corresponding to a motional ground

state); i.e.

$$K_n^{\ell m} \equiv K_{n,0}^{\ell m}, \quad K_n^m \equiv K_{n,0}^{m,0}, \quad K_{mn} \equiv K_{mn}^{0,0}, \quad K_n \equiv K_{n,0}^{0,0}, \quad K \equiv K_{0,0}^{0,0}. \quad (8)$$

For simplicity, we will also generally work in a gauge for which all two-body overlap integrals are real, such that $K_{mn}^{k\ell} = K_{mn}^{k\ell*} = K_{k\ell}^{mn}$. The existence of such a gauge is guaranteed by the analytic properties of the Wannier wavefunctions ϕ_{in} [48].

Current experiments with ^{87}Sr can prepare up to five atoms in the same (ground) orbital state on a single lattice site, and coherently address states with a single orbital excitation per lattice site [34]. At ultracold temperatures well below the non-interacting motional excitation energies $\Delta_n \equiv E_n - E_0$ for $n > 0$, atoms only occupy their motional ground state in the lattice. For this reason, it is common to map the description of these atoms onto a single-band Hubbard model that captures all dynamics within the subspace of motional ground states of non-interacting atoms, i.e. with wavefunctions $\phi_{i,0}$. Interactions, however, modify atoms' motional ground-state wavefunctions. The true motional ground state of a collection of interacting atoms is then an admixture of the non-interacting motional eigenstates, and a naive Hubbard model that assumes atomic wavefunctions $\phi_{i,0}$ will fail to reproduce the interacting atoms' orbital excitation spectrum. Formally, corrections to the spectrum of interacting atoms can be accounted for by a perturbative treatment of far-off-resonant terms in the interaction Hamiltonian of (7) that create atoms in excited motional states, e.g. $\sim \hat{c}_{n\mu s}^\dagger \hat{c}_{0,\nu t}^\dagger \hat{c}_{0,\nu r} \hat{c}_{0,\mu q}$ with $n > 0$. These corrections can be understood through interaction-induced *virtual* occupation of higher bands (i.e. excited motional states), which becomes relevant as more atoms occupy the same lattice site, such that their interaction energy becomes non-negligible compared to the motional excitation energies Δ_n .

In order to recast interaction-induced modifications to orbital excitation spectra as corrections to the simple Hubbard model (i.e. computed using the non-interacting ground-state wavefunctions $\phi_{i,0}$), we develop a low-energy effective theory of interacting AEAs in a deep lattice. To simplify our theory, we assume that any N atoms on a single lattice site occupy distinct nuclear spin states. This assumption applies for any experimental protocol in which all atoms are initially prepared in their orbital and motional ground states (as e.g. in ref. [34]). In this case, multiple occupation of a single nuclear spin state on any given lattice site is initially forbidden by fermionic statistics. Subsequent violation of this condition cannot occur in the absence of inter-site effects or hyperfine coupling between nuclear spin

states, as is the case of the experiment in ref. [34].

Our low-energy effective theory exhibits $SU(N)$ -symmetric multi-body interactions, such that the effective interaction Hamiltonian can be written in the form

$$H_{\text{int}}^{\text{eff}} = \sum_{M=2}^{2I+1} \sum_{p \geq 1} H_M^{(p)}, \quad (9)$$

where $H_M^{(p)}$ is an M -body Hamiltonian of order p in the coupling constants G_X , and I is the total nuclear spin of each atom (e.g. $I = 9/2$ for ^{87}Sr). The sum terminates at $2I + 1$ because this is the largest number of atoms which may initially occupy a single lattice site. We explicitly compute all M -body Hamiltonians $H_M \equiv \sum_p H_M^{(p)}$ through order $p = 3$, yielding effective two-, three-, and four-body interactions. To (i) facilitate a comparison with the experimental measurements of many-body orbital excitation spectra performed in ref. [34] and (ii) characterize the low-lying excitations in our effective theory, we additionally restrict the multi-body Hamiltonians H_M to states with at most one orbital excitation per lattice site. Under this restriction, we find that the $SU(N)$ symmetry of atomic collisions allows us to express all multi-body Hamiltonians in the simple form

$$H_M = \sum_{\{\mu_j\}=M} H_2^{(\mu_1, \mu_2)} \prod_{\alpha=3}^M \hat{n}_{\mu_\alpha, g}, \quad (10)$$

where $H_2^{(\mu_1, \mu_2)}$ is a two-body Hamiltonian addressing atoms with nuclear spin μ_1, μ_2 ; and $\hat{n}_{\mu s} = \hat{c}_{\mu s}^\dagger \hat{c}_{\mu s}$ is a number operator for atoms with nuclear state μ and orbital state s . The sum in (10) is performed over all choices of nuclear spins μ_j with $j = 1, 2, \dots, M$ for which all μ_j are distinct, or equivalently all choices of μ_j for which the set $\{\mu_j\}$ contains M elements, for a total of $\binom{2I+1}{M} \times (M!)$ nuclear spin combinations. The key feature of the M -body interactions in (10) is that they ultimately take the same form as two-body interactions, but with the addition of $M - 2$ spectator atoms. This form is a direct consequence of the $SU(N)$ symmetry of underlying two-body interactions.

III. LOW-ENERGY EFFECTIVE THEORY

The net Hamiltonian $H = H_0 + H_{\text{int}}$ for interacting AEAs on a lattice is not diagonal with respect to single-particle motional state indices (e.g. $n \in \mathbb{N}_0^3$). The problem of determining interacting atoms' orbital excitation spectrum therefore nominally involves all atomic motional degrees of freedom. At zero temperature, however, each orbital state of a collection

of interacting atoms is associated with a single motional ground state. In order to compute an orbital excitation spectrum at zero temperature, in principle we need to identify this motional ground state. We can then ignore all excited motional states, which will be neither thermally occupied nor externally interrogated. Such a procedure would drastically reduce the dimensionality of the Hilbert space necessary to describe the atoms, thereby greatly simplifying any description of the atoms' orbital spectrum and internal (i.e. nuclear and orbital) dynamics. In practice, however, identifying the motional ground states of interacting atoms and writing down a Hamiltonian restricted to this subspace is a very difficult process to carry out analytically.

We denote the motional ground-state subspace of the non-interacting Hamiltonian H_0 by $\mathcal{H}_{\text{ground}}^{\text{single}}$, and the motional ground-state subspace of the interacting Hamiltonian $H = H_0 + H_{\text{int}}$ by $\mathcal{H}_{\text{ground}}^{\text{multi}}$. That is, all atomic wavefunctions for states within $\mathcal{H}_{\text{ground}}^{\text{single}}$ are described by $\phi_{i,0}$, while the atomic wavefunctions for states within $\mathcal{H}_{\text{ground}}^{\text{multi}}$ are generally unknown, and are in principle determined by minimizing the energy of a state with respect to its motional degrees of freedom. Both $\mathcal{H}_{\text{ground}}^{\text{single}}$ and $\mathcal{H}_{\text{ground}}^{\text{multi}}$ are subspaces of the full Hilbert space $\mathcal{H}_{\text{full}}$. When interactions are sufficiently weak compared to the spectral gap Δ between $\mathcal{H}_{\text{ground}}^{\text{single}}$ and its orthogonal complement $\mathcal{H}_{\text{full}} \setminus \mathcal{H}_{\text{ground}}^{\text{single}}$, one can identify a particular unitary operator U (acting on the full Hilbert space $\mathcal{H}_{\text{full}}$) which rotates $\mathcal{H}_{\text{ground}}^{\text{multi}}$ into $\mathcal{H}_{\text{ground}}^{\text{single}}$ [49]. This unitary U can be used to construct an *effective Hamiltonian* $H_{\text{eff}} = UHU^\dagger$ with two key properties: (i) H_{eff} is diagonal in the same (known) basis as the non-interacting Hamiltonian H_0 , and (ii) the spectrum of H_{eff} on $\mathcal{H}_{\text{ground}}^{\text{single}}$ is identical to that of the interacting Hamiltonian H on $\mathcal{H}_{\text{ground}}^{\text{multi}}$. The use of an effective Hamiltonian H_{eff} thus overcomes the need to identify $\mathcal{H}_{\text{ground}}^{\text{multi}}$ in order to compute the orbital spectrum of H at zero temperature. This method for constructing an effective theory is commonly known as the Schrieffer-Wolff transformation, named after the authors of its celebrated application in relating the Anderson and Kondo models of magnetic impurities in metals [50].

Using the machinery developed in ref. [49] for performing a rotation between low-energy subspaces of a perturbed (i.e. interacting) and unperturbed (i.e. non-interacting) Hamiltonian, we derive an expansion for an effective interaction Hamiltonian $H_{\text{int}}^{\text{eff}}$ in terms two-body interaction Hamiltonian H_{int} (see Appendix A). This expansion takes the form

$$H_{\text{int}}^{\text{eff}} = \sum_{p \geq 1} H_{\text{int}}^{(p)}, \quad (11)$$

where $H_{\text{int}}^{(p)}$ is order p in H_{int} . Letting $\mathcal{E}_0 \equiv \mathcal{H}_{\text{full}} \setminus \mathcal{H}_{\text{ground}}^{\text{single}}$ denote the orthogonal complement of $\mathcal{H}_{\text{ground}}^{\text{single}}$ (i.e. \mathcal{E}_0 is the space of all states with at least one atom in an excited motional state), $\mathcal{B}_0(\mathcal{E}_0)$ denote an eigenbasis of \mathcal{E}_0 with respect to the single-particle Hamiltonian H_0 , and E_α denote the motional energy (with respect to H_0) of a state $|\alpha\rangle \in \mathcal{E}_0$ relative to the corresponding motional ground-state energy, we define the operator

$$\mathcal{I} \equiv \sum_{|\alpha\rangle \in \mathcal{B}_0(\mathcal{E}_0)} \frac{|\alpha\rangle\langle\alpha|}{E_\alpha}, \quad (12)$$

which sums over projections onto excited states with corresponding energetic suppression factors. The operator \mathcal{I} together with the projector \mathcal{P}_0 onto $\mathcal{H}_{\text{ground}}^{\text{single}}$ allows us concisely write the first few terms in (11) as

$$H_{\text{int}}^{(1)} = \mathcal{P}_0 H_{\text{int}} \mathcal{P}_0, \quad H_{\text{int}}^{(2)} = -\mathcal{P}_0 H_{\text{int}} \mathcal{I} H_{\text{int}} \mathcal{P}_0, \quad (13)$$

$$H_{\text{int}}^{(3)} = \mathcal{P}_0 H_{\text{int}} \mathcal{I} H_{\text{int}} \mathcal{I} H_{\text{int}} \mathcal{P}_0 - \frac{1}{2} [\mathcal{P}_0 H_{\text{int}} \mathcal{P}_0, \mathcal{P}_0 H_{\text{int}} \mathcal{I}^2 H_{\text{int}} \mathcal{P}_0]_+, \quad (14)$$

where $[X, Y]_+ \equiv XY + YX$. Writing down a single-band Hubbard model that simply neglects excited atomic motional states and uses H_{int} directly to describe the orbital spectrum of interacting atoms is thus equivalent to truncating our expansion for $H_{\text{int}}^{\text{eff}}$ at first order. In addition to this first order term, the expansion involves *effective corrections* to the action of H_{int} on the non-interacting motional ground states (i.e. on $\mathcal{H}_{\text{ground}}^{\text{single}}$) in the form of higher-order terms with *intermediate* or *virtual occupation* of excited states, manifest in \mathcal{I} .

Substituting the definition of \mathcal{I} into (13)-(14) yields expressions that are highly reminiscent of standard non-degenerate perturbation theory in quantum mechanics, but which nonetheless exhibit crucial differences. The first, and most obvious difference is that these expressions are operator equations, and that the sums over virtual states are performed over a basis for the orthogonal complement of the subspace $\mathcal{H}_{\text{ground}}^{\text{single}}$, rather than a basis for the orthogonal complement of a single state, as in non-degenerate perturbation theory. Second, the non-degeneracy condition in standard perturbation theory is here elevated to a restriction on the magnitude of the perturbation H_{int} relative to the spectral gap Δ of the non-interacting Hamiltonian H_0 between $\mathcal{H}_{\text{ground}}^{\text{single}}$ and the excited subspace \mathcal{E}_0 . Specifically, the validity of (13)-(14) is conditional only on $\|H_{\text{int}}\| \leq \Delta/2$, where $\|X\| \equiv \max_{|\psi\rangle \in \mathcal{H}} \sqrt{\langle\psi|X^\dagger X|\psi\rangle}$ is the operator norm, with no restrictions on spectral gaps or degeneracies within $\mathcal{H}_{\text{ground}}^{\text{single}}$ [49, 51].

Finally, the effective theory involves no corrections to the non-interacting many-body energy eigenstates; the purpose of constructing the effective Hamiltonian $H_{\text{eff}} = H_0 + H_{\text{int}}^{\text{eff}}$ is to reproduce, on the known eigenstates of the non-interacting Hamiltonian H_0 within $\mathcal{H}_{\text{ground}}^{\text{single}}$, the spectrum of the interacting Hamiltonian $H = H_0 + H_{\text{int}}$ on $\mathcal{H}_{\text{ground}}^{\text{multi}}$. “Correcting” the eigenstates of the non-interacting Hamiltonian H_0 on $\mathcal{H}_{\text{ground}}^{\text{single}}$ thus invalidates the effective theory.

As a last comment, we note that our chosen method for constructing an effective Hamiltonian is distinct from adiabatic elimination methods which are commonly used in the atomic physics and quantum optics communities to develop effective theories for e.g. the low-lying levels of a Lambda system [52–55]. Unlike the perturbative, but exact Schieffer-Wolff transformation, adiabatic elimination methods use approximations which rely on the fast dynamics of excited states. While generally reasonable, these approximations must be made carefully to avoid potential problems with self-consistency (see section 3 of ref. [52]), and yield no obvious or straightforward means to compute effective corrections beyond second order in the couplings between low- and high-energy sectors of a Hilbert space [53–55]. While at least one attempt at systematically computing higher-order corrections in the framework of adiabatic elimination has recently been made [55], the resulting expressions do not lend themselves as nicely to analytical treatment, and were in any case found by the authors to be equivalent to a Schieffer-Wolff transformation.

A. Diagrammatic representation of effective Hamiltonians

The form of the bare two-body interaction Hamiltonian H_{int} in (7) motivates a diagrammatic representation of terms in the effective Hamiltonian H_{eff} in (11), similarly to the diagrams used to represent elements of the scattering matrix in standard quantum field theory. Effective M -body interaction terms at order p in H_{int} can be represented by directed graphs containing p vertices with degree greater than one, which we call *internal vertices*. Each internal vertex and its associated edges correspond respectively to a coupling constant and the associated field operators in H_{int} . An example 2-vertex diagram representing an effective 3-body interaction term is provided in figure 1. All diagrams are read from left to right to construct a sequence of operators from right to left; the internal vertices of a diagram are thus strictly ordered, with the n -th internal vertex from the left corresponding to the n -th

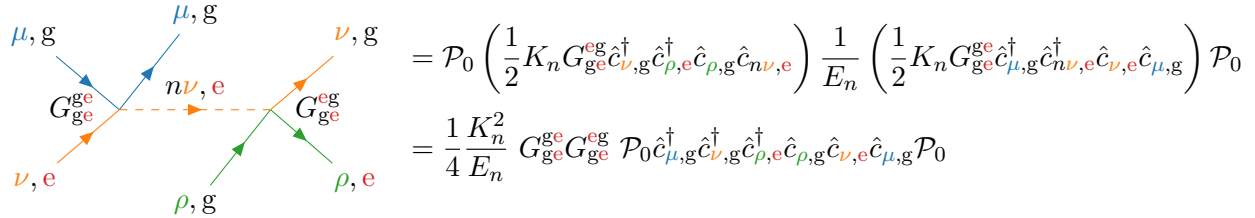


FIG. 1. An example second-order diagram and the corresponding three-body interaction term in $H_{\text{int}}^{(2)}$, with $n > 0$ and $\hat{c}_{\mu s} \equiv \hat{c}_{0, \mu s}$. Diagrams are read from left to right to construct a sequence of operators from right to left. Solid (dashed) lines represent field operators acting on the lowest (arbitrary) motional states. For the sake of presentation, this diagram has colors associated with nuclear spin and orbital states, an arrow on each line to emphasize that they are directed left-to-right, and an explicit coupling constant written next to each vertex; we will generally not include these features, as they are not necessary to uniquely identify the term represented by a diagram. We will also drop explicit appearances of the ground-state projector \mathcal{P}_0 in our expressions, with the understanding that the low-energy effective theory implicitly addresses only non-interacting motional ground states.

interaction Hamiltonian H_{int} from the right in (13) or (14). Solid (dashed) lines represent field operators acting on the lowest (arbitrary) motional states. Spatial overlap factors at each vertex are determined by the motional states of the edges which connect to (i.e. field operators associated with) that vertex. While it is possible to construct explicit rules for determining the energetic suppression factors (i.e. from \mathcal{I}) of the term represented by a diagram, these factors are most easily determined by examination of the effective Hamiltonians in (13) and (14).

The diagram in figure 1 explicitly labels all edges with indices of the corresponding field operators, but in general we may suppress these indices, in which case the diagram includes a sum over the suppressed indices. These sums are performed over all allowed values of the suppressed indices, with the restriction that virtual states (i.e. vertical slices of the diagram between internal vertices) represented with dashed lines must have at least one motional excitation. While we include factors of $1/2$ from H_{int} as expressed in (7) in the definition of a diagram, in all but the two-body case these factors of $1/2$ will be cancelled out by corresponding symmetry factors, i.e. the appearance of duplicate diagrams which are equal up to a relabeling of indices (see Appendix B). The explicit signs and factor of $1/2$ which appear in the effective Hamiltonians in (13) and (14) are not included in the definition of a

diagram, and must be kept track of manually.

B. Effective two-body interactions and renormalization

The effective two-body Hamiltonian in (11) has contributions at all orders in the coupling constants, and can be expanded in the form

$$H_2 = \text{diagram 1} - \text{diagram 2} + \text{diagram 3} + \dots \equiv \text{diagram 4}, \quad (15)$$

where the blob on the right schematically represents the net effective two-body interaction. On physical grounds, the net two-body interaction must clearly be finite, but individual sums over excited states in the loop diagrams of (15) may generally diverge [35]. These divergences ultimately appear due to our use of effective field theory to describe interatomic interactions in (2), (5), and (7), rather than a detailed microscopic description of two-atom scattering. Divergences of this sort are a generic feature of field theories, and can be dealt with using standard techniques such as renormalization. We therefore renormalize our coupling constants by introducing counter-terms \tilde{G}_X into the interaction Hamiltonian.

The introduction of counter-terms is merely a formal decomposition of the “bare” coupling constants G_X^{bare} that are used in (15) as $G_X^{\text{bare}} = G_X + \tilde{G}_X$. In performing such a decomposition, we are free to choose the values of G_X , which in turn fixes the values of $\tilde{G}_X \equiv G_X^{\text{bare}} - G_X$. For convenience, we can choose the values of G_X to be those of the net effective coupling constants on the right-hand side of (15). Representing the new coupling constants G_X by regular vertices and the counter-terms \tilde{G}_X by a crossed dot (i.e. \otimes), this choice leads to the *renormalization condition*

$$\text{diagram 1} + \text{diagram 5} - \text{diagram 2} + \dots = \text{diagram 1}. \quad (16)$$

This renormalization condition has the benefit of allowing us to express effective two-body interactions simply in terms of net effective two-body coupling constants, rather than in terms of long sums at all order of the bare coupling constants. By construction, the counter-terms we have introduced exactly cancel all terms beyond leading order in (15), which implies that the effective two-body interaction Hamiltonian is simply

$$H_2 = \text{diagram 1} = \frac{1}{2} \alpha_2^{(1)} \sum_{|\{\mu, \nu\}|=2} G_{st}^{qr} \hat{c}_{\mu s}^\dagger \hat{c}_{\nu t}^\dagger \hat{c}_{\nu r} \hat{c}_{\mu q}, \quad (17)$$

where for consistency with existing literature [35] we define $\alpha_2^{(1)} \equiv K$ as the overlap integral between two atoms occupying non-interacting motional ground states.

Before moving on to consider effective three-body interactions, there are a few comments we must make concerning renormalization and the result in (17). First, the effective two-body interaction H_2 in (17) takes the same form as the bare two-body interaction H_{int} in (7), but without excited motional states, and with renormalized coupling constants. Our choice of renormalization scheme, while convenient for the analytical development of a low-energy effective theory, no longer allows us to use the coupling constants G_X as defined by the free-space scattering lengths a_X in (3) to compute interaction energies. The renormalization condition in (16) explicitly fixes G_X to the net effective coupling constants in any given setting. Instead of using free-space coupling constants to compute interaction energies in a lattice, we must therefore first compute the effective coupling constants $G_X^{\text{lattice}}(\mathcal{U})$, which now depend on the lattice depth \mathcal{U} , and in turn use these effective coupling constants to compute interaction energies. We discuss the calculation of effective coupling constants in Appendix C.

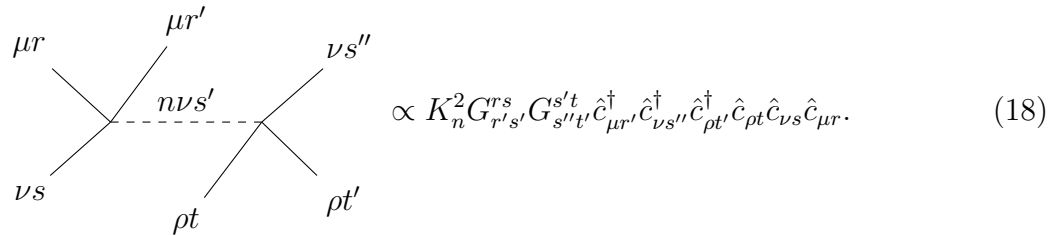
Second, the renormalization condition in (16) implies that the counter terms \tilde{G}_X are second order in the coupling constants G_X , i.e. $\tilde{G}_X \sim G_X^2$. Although the effective Hamiltonian expansions in (13) and (14) are organized in powers of the interaction Hamiltonian H_{int} , the couplings G_X are the “small” parameters in which we can formally organize a perturbation theory; more specifically, the formally small quantities organizing our perturbation theory are two-body ground-state interaction energies (proportional to the couplings G_X) divided by the spectral gap of the single-atom Hamiltonian H_0 (see Appendix F). If M atoms can only couple through terms represented by a p -vertex diagrams for $p \geq p_M^{\text{min}}$, then the leading order contribution to M -body interactions is order p_M^{min} in the couplings G_X . If the same p_M^{min} -vertex diagrams involve any counter-terms, however, then these diagrams are at least order $p_M^{\text{min}} + 1$ in the couplings G_X . Counter-terms therefore only appear at next-to-leading order (NLO) in the calculation of effective M -body interactions.

Finally, our result in (17) neglects the effect of momentum-dependent two-body scattering. When the effective range of interactions is comparable to the scattering lengths a_X , as is the case for ultracold ^{87}Sr , these momentum-dependent effects are third order in the coupling constants G_X . Just as the $\mathcal{O}(G^2)$ counter-terms do not affect M -body interactions until next-to-leading order (NLO), the $\mathcal{O}(G^3)$ momentum-dependent terms do not come into

play until next-next-leading order (NNLO). Given that we develop our low-energy effective theory through third order in the coupling constants, these interactions will not appear in any of our three- and four-body calculations, but they do need to be considered in the calculation of pair-wise interaction energies. The primary interest of our work, however, concerns effective M -body interactions for $M \geq 3$; we therefore defer the calculation of momentum-dependent two-body interactions to Appendix D.

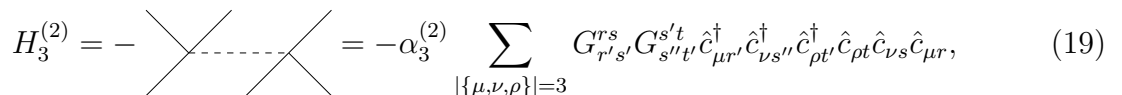
C. Effective three-body interactions at second order

Our theory of effective multi-body interactions assumes no non-universal contribution to the three-body interaction energy, which is to say that we assume the absence of real (as opposed to effective), bare three-body interactions. Consequently, three-body interactions do not appear until second order in the coupling constants of the effective theory, in the expansion of $H_{\text{int}}^{(2)}$ in (13). The virtual state of three-body terms in $H_{\text{int}}^{(2)}$ cannot have two atoms in excited motional states, as otherwise the second application of H_{int} in $H_{\text{int}}^{(2)}$ would have to address both of these atoms to bring them back down to the ground state, resulting in a two-body process as in the second diagram of (15). All second-order three-body terms must therefore have only one excited atom in the virtual state, and take the form



$$\propto K_n^2 G_{r's'}^{rs} G_{s''t'}^{s't} \hat{c}_{\mu r'}^\dagger \hat{c}_{\nu s''}^\dagger \hat{c}_{\rho t'}^\dagger \hat{c}_{\rho t} \hat{c}_{\nu s} \hat{c}_{\mu r}. \quad (18)$$

Unlike for the two-body diagram in (17), the explicit factors of $1/2$ which appear in the bare two-body Hamiltonian H_{int} in (7) are now cancelled out by symmetry factors which account for duplicate diagrams; this cancellation will generally occur for all connected M -body diagrams with $M > 2$ (see Appendix B). The net effective three-body interaction Hamiltonian at second order is then given by the sum over all diagrams of the form in (18), i.e.



$$H_3^{(2)} = - \text{Diagram} = -\alpha_3^{(2)} \sum_{|\{\mu, \nu, \rho\}|=3} G_{r's'}^{rs} G_{s''t'}^{s't} \hat{c}_{\mu r'}^\dagger \hat{c}_{\nu s''}^\dagger \hat{c}_{\rho t'}^\dagger \hat{c}_{\rho t} \hat{c}_{\nu s} \hat{c}_{\mu r}, \quad (19)$$

where $\alpha_3^{(2)} \equiv \sum_{n>0} K_n^2/E_n$, and the preceding minus sign is as prescribed by $H_{\text{int}}^{(2)}$ in (13).

D. Effective three-body interactions at third order

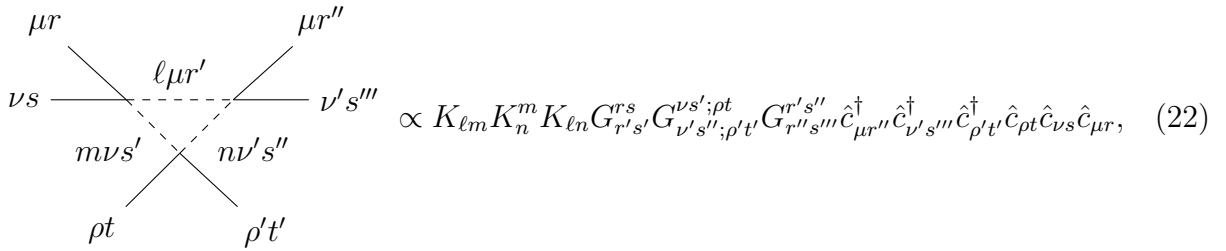
The third-order effective interaction Hamiltonian $H_{\text{int}}^{(3)}$ in (14) contains both three- and four-body terms. To compactly enumerate and evaluate all three-body diagrams at third order, we introduce an expanded coupling symbol

$$G_{\rho s; \sigma t}^{\mu q; \nu r} \equiv \begin{cases} G_{st}^{qr} & (\mu, \nu) = (\rho, \sigma) \\ -G_{ts}^{qr} & (\mu, \nu) = (\sigma, \rho) \\ 0 & \text{otherwise} \end{cases} \quad (20)$$

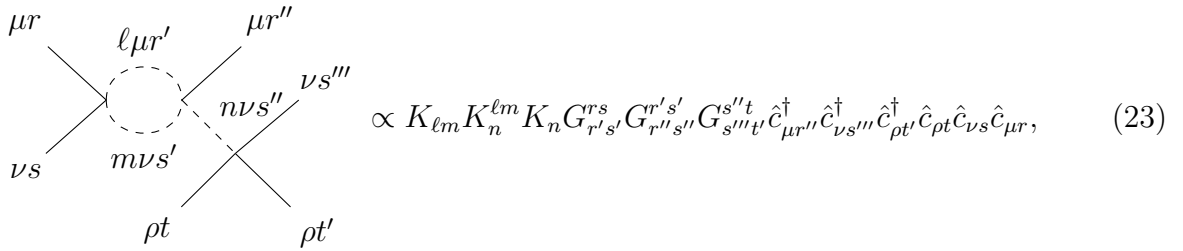
for more general $(\mu, q) + (\nu, r) \leftrightarrow (\rho, s) + (\sigma, t)$ coupling induced by terms proportional to $\hat{c}_{\rho s}^\dagger \hat{c}_{\sigma t}^\dagger \hat{c}_{\nu r} \hat{c}_{\mu q}$. The minus sign in (20) accounts for fermionic statistics: if $(\mu, \nu) = (\sigma, \rho)$, then we are considering a term of the form

$$G_{\nu s; \mu t}^{\mu q; \nu r} \hat{c}_{\nu s}^\dagger \hat{c}_{\mu t}^\dagger \hat{c}_{\nu r} \hat{c}_{\mu q} = -G_{ts}^{qr} \hat{c}_{\nu s}^\dagger \hat{c}_{\mu t}^\dagger \hat{c}_{\nu r} \hat{c}_{\mu q} = G_{ts}^{qr} \hat{c}_{\mu t}^\dagger \hat{c}_{\nu s}^\dagger \hat{c}_{\nu r} \hat{c}_{\mu q}. \quad (21)$$

At the cost of introducing an additional sum over new nuclear spin indices, the expanded coupling symbol allows us to collect together diagrams which have the same graph topology, but represent different matrix elements of the effective Hamiltonian due to the exchange of nuclear spins at a vertex. The third order three-body diagrams in $H_{\text{int}}^{(3)}$ are then



$$\propto K_{\ell m} K_n^m K_{\ell n} G_{r' s'}^{r s} G_{\nu' s''; \rho t}^{\nu s'; \rho t} G_{r'' s''}^{r' s''} \hat{c}_{\mu r''}^\dagger \hat{c}_{\nu' s''}^\dagger \hat{c}_{\rho' t'}^\dagger \hat{c}_{\rho t} \hat{c}_{\nu s} \hat{c}_{\mu r}, \quad (22)$$



$$\propto K_{\ell m} K_n^{\ell m} K_n G_{r' s'}^{r s} G_{r'' s''}^{r' s''} G_{s'' t}^{s'' t} \hat{c}_{\mu r''}^\dagger \hat{c}_{\nu s''}^\dagger \hat{c}_{\rho' t'}^\dagger \hat{c}_{\rho t} \hat{c}_{\nu s} \hat{c}_{\mu r}, \quad (23)$$

and the mirror image of (23). As prescribed by $H_{\text{int}}^{(3)}$ in (14), these diagrams have an associated minus sign if they contain only one excited virtual state, and a factor of 1/2 if they contain a virtual ground state. Remembering that counter-terms are $\mathcal{O}(G^2)$, there are

additionally two third-order three-body diagrams in $H_{\text{int}}^{(2)}$, namely

$$\propto K_n^2 \tilde{G}_{r's'}^{rs} G_{s''t'}^{s't} \hat{c}_{\mu r'}^\dagger \hat{c}_{\nu s''}^\dagger \hat{c}_{\rho t'}^\dagger \hat{c}_{\rho t} \hat{c}_{\nu s} \hat{c}_{\mu r} \quad (24)$$

and its mirror image, where \tilde{G}_{st}^{qr} is equal to the counter-term associated with G_{st}^{qr} .

The net contribution to the third-order three-body interaction Hamiltonian from three-particle-loop diagrams of the form in (22) is

$$= \left(\alpha_{3,1}^{(3)} - \alpha_5^{(3)} \right) \mathcal{H}_{3,1}^{(3)}, \quad (25)$$

where

$$\alpha_{3,1}^{(3)} \equiv \sum_{\substack{\ell+m>0 \\ \ell+n>0}} \frac{K_{\ell m} K_n^m K_{\ell n}}{E_{\ell m} E_{\ell n}}, \quad \alpha_5^{(3)} \equiv K \sum_{n>0} \frac{K_n^2}{E_n^2}, \quad (26)$$

and

$$\mathcal{H}_{3,1}^{(3)} \equiv \sum_{|\{\mu, \nu, \rho\}|=3} G_{r's'}^{rs} G_{\nu's''\rho't'}^{\nu s' \rho t} G_{r''s''m}^{r's''} \hat{c}_{\mu r''}^\dagger \hat{c}_{\nu's''m}^\dagger \hat{c}_{\rho't'}^\dagger \hat{c}_{\rho t} \hat{c}_{\nu s} \hat{c}_{\mu r}. \quad (27)$$

Even though this contribution comes from loop diagrams, the factors $\alpha_{3,1}^{(3)}$ and $\alpha_5^{(3)}$ in (26) are finite. At large motional state indices n , atoms become free particles for which n essentially indexes discrete momentum states. These atoms thus have an energy which asymptotically scales as $E_n \sim n^2 \equiv n_x^2 + n_y^2 + n_z^2$. Furthermore, the oscillatory behavior of atomic wavefunctions with increasing motional state indices ℓ, m implies that the overlap integral $K_{\ell m}$ becomes sharply peaked at $\ell \approx m$ as ℓ and m get large. The asymptotic behavior of $\alpha_{3,1}^{(3)}$ at large ℓ, m, n is therefore

$$\alpha_{3,1}^{(3)} \sim \int \frac{d^3 \ell d^3 m d^3 n}{(\ell^2 + m^2)(\ell^2 + n^2)} \delta(\ell - m) \delta(\ell - n) \sim \int \frac{d^3 \ell}{\ell^4} \sim \int_{\ell_{\min}}^{\infty} \frac{d\ell}{\ell^2} \sim \frac{1}{\ell_{\min}}, \quad (28)$$

where in the last integral we changed to spherical coordinates, and ℓ_{\min}^2 is the minimum value of ℓ^2 for which (i) the energy $E_\ell \sim \ell^2$, and (ii) the integral expression in (28) is a good approximation to the corresponding sum in (26). Note that the introduction of ℓ_{\min} amounts to neglecting a finite number of terms in the sum over ℓ, m, n in (26), whose

contribution to the value of $\alpha_{3,1}^{(3)}$ is finite. Convergence of $\alpha_5^{(3)}$ is similarly guaranteed by the fact that the overlap integral K_n does not asymptotically grow with increasing n , such that $\alpha_5^{(3)}$ asymptotically behaves as

$$\alpha_5^{(3)} \sim \int \frac{d^3n}{n^4} \sim \int_{n_{\min}}^{\infty} \frac{dn}{n^2} \sim \frac{1}{n_{\min}}, \quad (29)$$

where again n_{\min} is defined similarly to ℓ_{\min} .

The sum over loop diagrams in (23), meanwhile, contains a divergence that must be cancelled out by the counter-terms in (24). To leading order in the coupling constants, the renormalization condition in (16) implies that

$$\text{Diagram with a cross and a central dot} = \text{Diagram with a dashed loop and a central dot}, \quad (30)$$

which can be expanded to find

$$K\tilde{G}_{r''s''}^{rs} = \sum_{\ell,m,r',s'} \frac{K_{\ell m}^2}{E_{\ell m}} G_{r's'}^{rs} G_{r''s''}^{r's'}. \quad (31)$$

In terms of ordinary coupling constants, the counter-term diagram in (24) is therefore

$$\text{Diagram with a cross and a dashed line} = \sum_{\ell,m,r',s'} \frac{K_{\ell m}^2 K_n^2}{K E_{\ell m} E_n} G_{r's'}^{rs} G_{r''s''}^{r's'} G_{s'''t'}^{s''t} \hat{c}_{\mu r''}^\dagger \hat{c}_{\nu s''}^\dagger \hat{c}_{\rho t'}^\dagger \hat{c}_{\rho t} \hat{c}_{\nu s} \hat{c}_{\mu r}. \quad (32)$$

Altogether, the contribution to the third-order three-body interaction Hamiltonian from loop diagrams of the form in (23) and counter-term diagrams of the form in (24) is

$$\begin{aligned} & \text{Diagram with a dashed loop} - \text{Diagram with a cross and a dashed line} - \frac{1}{2} \text{Diagram with a dashed loop} - \frac{1}{2} \text{Diagram with a solid loop} \\ & = \left(\alpha_{3,2}^{(3)} - \frac{1}{2} \alpha_{4,3}^{(3)} - \frac{1}{2} \alpha_5^{(3)} \right) \mathcal{H}_{3,2}^{(3)}, \end{aligned} \quad (33)$$

where

$$\alpha_{3,2}^{(3)} \equiv \sum_{\substack{\ell+m>0 \\ n>0}} \frac{K_{\ell m} K_n}{E_{\ell m} E_n} \left(K_n^{\ell m} - \frac{K_{\ell m} K_n}{K} \right), \quad \alpha_{4,3}^{(3)} \equiv K \sum_{m+n>0} \frac{K_{mn}^2}{E_{mn}^2}, \quad (34)$$

and

$$\mathcal{H}_{3,2}^{(3)} \equiv \sum_{|\{\mu,\nu,\rho\}|=3} G_{r's'}^{rs} G_{r''s''}^{r's'} G_{s'''t'}^{s''t} \hat{c}_{\mu r''}^\dagger \hat{c}_{\nu s''}^\dagger \hat{c}_{\rho t'}^\dagger \hat{c}_{\rho t} \hat{c}_{\nu s} \hat{c}_{\mu r}. \quad (35)$$

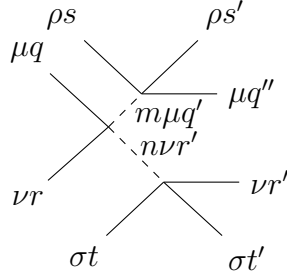
An equal contribution comes from the mirror images of these diagrams, such that the net third-order three-body interaction Hamiltonian is

$$H_3^{(3)} = \left(\alpha_{3,1}^{(3)} - \alpha_5^{(3)} \right) \mathcal{H}_{3,1}^{(3)} + \left(2\alpha_{3,2}^{(3)} - \alpha_{4,3}^{(3)} - \alpha_5^{(3)} \right) \mathcal{H}_{3,2}^{(3)}. \quad (36)$$

Note that the aforementioned divergence and its cancellation are buried in $\alpha_{3,2}^{(3)}$. Formally, this factor is calculated by imposing an ultraviolet cutoff Λ for the maximum values of motional state indices ℓ, m, n , and then taking the limit $\Lambda \rightarrow \infty$. This procedure ensures that there are no divergences in $\alpha_{3,2}^{(3)}$.

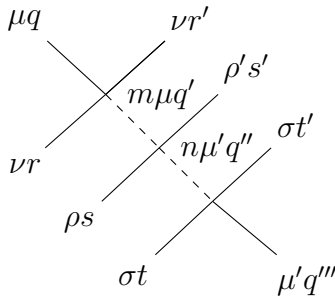
E. Effective four-body interactions at third order

At third order in the coupling constants, we have four-body terms of the form



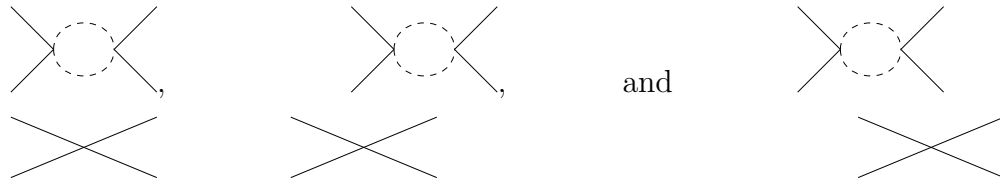
$$\propto K_{mn} K_m K_n G_{q'r'}^{qr} G_{q''s'}^{q's} G_{r''t'}^{r't} \hat{c}_{\mu q''}^\dagger \hat{c}_{\nu r''}^\dagger \hat{c}_{\rho s'}^\dagger \hat{c}_{\sigma t'}^\dagger \hat{c}_{\sigma t} \hat{c}_{\rho s} \hat{c}_{\nu r} \hat{c}_{\mu q} \quad (37)$$

and its mirror image, as well as



$$\propto K_m K_n^m K_n G_{q'r'}^{qr} G_{\mu'q''\rho's'}^{\mu q' \rho s} G_{q'''t'}^{q''t} \hat{c}_{\mu'q'''}^\dagger \hat{c}_{\nu r'}^\dagger \hat{c}_{\rho's'}^\dagger \hat{c}_{\sigma t'}^\dagger \hat{c}_{\sigma t} \hat{c}_{\rho s} \hat{c}_{\nu r} \hat{c}_{\mu q}. \quad (38)$$

As we are computing the leading-order contribution to effective four-body interactions, there are no counter-terms contributions. In principle, there is now also the possibility to make the disconnected diagrams of the form



$$\quad \quad \quad \text{and} \quad \quad \quad . \quad (39)$$

As prescribed by $H_{\text{int}}^{(3)}$ in (14), however, the second and third of these diagrams pick up a factor of $-1/2$, so the sum over disconnected diagrams vanishes.

The contribution to the third-order four-body interaction Hamiltonian from diagrams of the form in (37) is

$$\begin{array}{c} \diagup \quad \diagdown \\ \diagdown \quad \diagup \\ \text{---} \quad \text{---} \\ \diagdown \quad \diagup \\ \diagup \quad \diagdown \end{array} - \frac{1}{2} \begin{array}{c} \diagup \quad \diagdown \\ \diagdown \quad \diagup \\ \text{---} \quad \text{---} \\ \diagdown \quad \diagup \\ \diagup \quad \diagdown \end{array} = \left(\alpha_{4,1}^{(3)} - \frac{1}{2} \alpha_5^{(3)} \right) \mathcal{H}_{4,1}, \quad (40)$$

where

$$\alpha_{4,1}^{(3)} \equiv \sum_{\substack{m \geq 0 \\ n > 0}} \frac{K_{mn} K_m K_n}{E_{mn} E_n}, \quad (41)$$

and

$$\mathcal{H}_{4,1}^{(3)} \equiv \sum_{|\{\mu, \nu, \rho, \sigma\}|=4} G_{q'r'}^{qr} G_{q''s'}^{q's} G_{r''t'}^{r't} \hat{c}_{\mu q''}^\dagger \hat{c}_{\nu r''}^\dagger \hat{c}_{\rho s'}^\dagger \hat{c}_{\sigma t'}^\dagger \hat{c}_{\sigma t} \hat{c}_{\rho s} \hat{c}_{\nu r} \hat{c}_{\mu q}. \quad (42)$$

An equal contribution comes from the mirror images of these diagrams. The contribution from diagrams of the form in (38), meanwhile, is

$$\begin{array}{c} \diagdown \quad \diagup \\ \diagup \quad \diagdown \\ \text{---} \quad \text{---} \\ \diagup \quad \diagdown \\ \diagdown \quad \diagup \end{array} - \frac{1}{2} \begin{array}{c} \diagdown \quad \diagup \\ \diagup \quad \diagdown \\ \text{---} \quad \text{---} \\ \diagup \quad \diagdown \\ \diagdown \quad \diagup \end{array} - \frac{1}{2} \begin{array}{c} \diagdown \quad \diagup \\ \diagup \quad \diagdown \\ \text{---} \quad \text{---} \\ \diagup \quad \diagdown \\ \diagdown \quad \diagup \end{array} = \left(\alpha_{4,2}^{(3)} - \alpha_5^{(3)} \right) \mathcal{H}_{4,2}, \quad (43)$$

where

$$\alpha_{4,2}^{(3)} \equiv \sum_{m, n > 0} \frac{K_m K_n^m K_n}{E_m E_n}, \quad (44)$$

and

$$\mathcal{H}_{4,2}^{(3)} \equiv \sum_{|\{\mu, \nu, \rho, \sigma\}|=4} G_{q'r'}^{qr} G_{\mu'q''\rho's'}^{\mu q' \rho s} G_{q''t'}^{q''t} \hat{c}_{\mu' q''}^\dagger \hat{c}_{\nu' r'}^\dagger \hat{c}_{\rho' s'}^\dagger \hat{c}_{\sigma t'}^\dagger \hat{c}_{\sigma t} \hat{c}_{\rho s} \hat{c}_{\nu r} \hat{c}_{\mu q}. \quad (45)$$

The net third-order four-body interaction Hamiltonian is therefore

$$H_4^{(3)} = \left(2\alpha_{4,1}^{(3)} - \alpha_5^{(3)} \right) \mathcal{H}_{4,1}^{(3)} + \left(\alpha_{4,2}^{(3)} - \alpha_5^{(3)} \right) \mathcal{H}_{4,2}^{(3)}. \quad (46)$$

IV. LOW-EXCITATION HAMILTONIANS, EIGENSTATES, AND SPECTRA

Current experiments with ultracold ^{87}Sr on a lattice can coherently address ground states and single orbital excitations of up to five atoms per lattice site [34]. Due to the $\text{SU}(N)$ symmetry of inter-atomic interactions, manifest in the fact that all coupling constants are independent of nuclear spin, a restriction of the M -body Hamiltonians $H_M = \sum_p H_M^{(p)}$ to the subspace of experimentally addressed states takes the form

$$H_M = \sum_{\{|\mu_j\rangle\}=M} (U_{M,g} \hat{n}_{\mu_1,g} \hat{n}_{\mu_2,g} + U_{M,+} \hat{n}_{\mu_1,e} \hat{n}_{\mu_2,g} + U_{M,-} \hat{c}_{\mu_1,g}^\dagger \hat{c}_{\mu_2,e}^\dagger \hat{c}_{\mu_2,g} \hat{c}_{\mu_1,e}) \prod_{\alpha=3}^M \hat{n}_{\mu_\alpha,g}, \quad (47)$$

where $\hat{n}_{\mu s} \equiv \hat{c}_{\mu s}^\dagger \hat{c}_{\mu s}$ is a number operator, and the coefficients U_X can be determined from the coupling constants G_Y and prefactors $\alpha_Z^{(p)}$ of the effective M -body Hamiltonians derived in section III (see Appendix G). For a lattice with $N \geq M$ atoms occupying nuclear spins $\mathcal{N} = \{\mu_j\}$ for $j = 1, 2, \dots, N$, the M -body Hamiltonian H_M has a single ground state $|\mathcal{N}, 0\rangle$, and a singly-excited state $|\mathcal{N}, +\rangle$ which is fully symmetric in the orbital degrees of freedom; these states are

$$|\mathcal{N}, 0\rangle \equiv \left(\prod_{\mu \in \mathcal{N}} \hat{c}_{\mu,g}^\dagger \right) |\text{vacuum}\rangle, \quad |\mathcal{N}, +\rangle \equiv \frac{1}{\sqrt{N}} \sum_{\mu \in \mathcal{N}} \hat{c}_{\mu,e}^\dagger \hat{c}_{\mu,g} |\mathcal{N}, 0\rangle. \quad (48)$$

As these states are fully symmetric in their orbital degrees of freedom, they are anti-symmetric in their nuclear spin degrees of freedom, forming an $\text{SU}(N)$ singlet. Furthermore, the symmetric state is particularly interesting as its orbital degrees of freedom form an N -body entangled W state, which belongs to a special class of multi-partite entangled states that are robust against disposal or loss of particles. This state thus constitutes an important resource for many quantum information processing and quantum communication tasks [56].

In addition to the states in (48), the multi-body Hamiltonian H_M in (47) has an $(N - 1)$ -fold degenerate excited-state eigenspace which is asymmetric in the orbital degrees of freedom, spanned by the states

$$|\mathcal{N}, -, j\rangle \equiv \frac{1}{\sqrt{2}} \left(\hat{c}_{\mu_1,e}^\dagger \hat{c}_{\mu_1,g} - \hat{c}_{\mu_j,e}^\dagger \hat{c}_{\mu_j,g} \right) |\mathcal{N}, 0\rangle \quad (49)$$

for $j = 2, \dots, N$. If $N > 2$, the asymmetric states are not separable in their orbital and nuclear spin degrees of freedom. An important feature of the excited states in (48) and (49) is that they are entirely independent of M , which implies that the effect of multi-body

TABLE I. Low-excitation eigenvalues of M -body Hamiltonians H_M . Many-body energy eigenstates are labeled by the nuclear spins they occupy (i.e. \mathcal{N} with $N \equiv |\mathcal{N}|$) and whether they are in an orbital ground (0), singly-excited symmetric (+), or singly-excited asymmetric (-) state. The corresponding N -body eigenvalues $E_{NX}^{(M)}$ of H_M are given in terms of the coefficients U_{MX} as appearing in (47) (first three rows), in addition to the M -body eigenvalues $E_{MX}^{(M)}$ (last three rows).

Eigenstate	H_M eigenvalue ($M \leq N$)
$ \mathcal{N}, 0\rangle$	$M! \binom{N}{M} U_{M,g}$
$ \mathcal{N}, +\rangle$	$M! \binom{N-1}{M} U_{M,g} + (M-1)! \binom{N-1}{M-1} (U_{M,+} + U_{M,-})$
$ \mathcal{N}, -\rangle$	$M! \binom{N-1}{M} U_{M,g} + (M-1)! \binom{N-1}{M-1} U_{M,+} - (M-2)! \binom{N-2}{M-2} U_{M,-}$
$ \mathcal{N}, 0\rangle$	$\binom{N}{M} E_{M,0}^{(M)}$
$ \mathcal{N}, +\rangle$	$\binom{N-1}{M} E_{M,0}^{(M)} + \binom{N-1}{M-1} E_{M,+}^{(M)}$
$ \mathcal{N}, -\rangle$	$\binom{N-1}{M} E_{M,0}^{(M)} + M^{-1} \left[\binom{N-1}{M-1} - \binom{N-2}{M-2} \right] E_{M,+}^{(M)} + \left[(1 - M^{-1}) \binom{N-1}{M-1} + M^{-1} \binom{N-2}{M-2} \right] E_{M,-}^{(M)}$

interactions is simply to modify the many-body atomic energy spectra without affecting the energy eigenstates. The eigenvalues $E_{NX}^{(M)} = \langle \mathcal{N}X | H_M | \mathcal{N}X \rangle$ of H_M associated with each of the eigenstates in (48) and (49) are provided in table I, both in terms of the coefficients U_{MX} of H_M as expressed in (47) and the M -body eigenvalues $E_{MX}^{(M)}$. Due to the $SU(N)$ symmetry of the multi-body Hamiltonian H_M , the eigenvalues $E_{NX}^{(M)}$ depend on the number of nuclear spins on a lattice site, N , but not on the actual nuclear spins $\mu \in \mathcal{N}$ which are occupied. The total N -body interaction energies E_{NX} are given in terms of the M -body eigenvalues $E_{NX}^{(M)}$ by $E_{NX} = \sum_M E_{NX}^{(M)}$.

A. Many-body state spectroscopy

Spectroscopic interrogation is a powerful means to probe the internal structure and dynamics of a system under examination. Consequently, we consider Rabi spectroscopy of the low-lying energy eigenstates in multiply-occupied lattice sites. If we interrogate a lattice site by a laser red-detuned by Δ from the single-atom orbital state excitation energy, we realize the Hamiltonian

$$H_{\text{Rabi}} = \sum_X E_X \mathcal{P}_X + \sum_\mu (\Delta T_\mu^z + \Omega_\mu T_\mu^x), \quad (50)$$

where E_X is an eigenvalue of the effective interaction Hamiltonian $H_{\text{int}}^{\text{eff}}$, \mathcal{P}_X is a projector onto the corresponding eigenspace, and

$$T_\mu^z \equiv \frac{1}{2} (\hat{c}_{\mu,e}^\dagger \hat{c}_{\mu,e} - \hat{c}_{\mu,g}^\dagger \hat{c}_{\mu,g}), \quad T_\mu^x \equiv \frac{1}{2} (\hat{c}_{\mu,e}^\dagger \hat{c}_{\mu,g} + \hat{c}_{\mu,g}^\dagger \hat{c}_{\mu,e}), \quad (51)$$

are single-atom pseudospin operators. The Rabi frequency Ω_μ is proportional to the Clebsch-Gordan coefficient $\langle I, \mu; 1, 0 | I, \mu \rangle \propto \mu$ for a photon-induced nuclear-spin-conserving orbital state transition of an atom with nuclear spin μ . We therefore define the “bare” Rabi frequency $\Omega_0 \equiv \Omega_\mu/\mu$ to explicitly factor out dependence on nuclear spins μ .

Consider now a single lattice site in the orbital ground state $|\mathcal{N}, 0\rangle$ with nuclear spins $\mathcal{N} \equiv \{\mu_j\}$ for $j = 1, 2, \dots, N$. If we red-detune the interrogation laser by δ from a many-body orbital state excitation energy, i.e. set $\Delta = \Delta_{NX} - \delta$ for $\Delta_{NX} \equiv E_{NX} - E_{N,0}$ and $X \in \{+, -\}$, then in the subspace of the target states $\{|\mathcal{N}, 0\rangle, |\mathcal{N}X\rangle\}$ the Hamiltonian in (50) becomes

$$H_{NX} = \delta S_{NX}^z + \Omega_{NX} S_{NX}^x, \quad (52)$$

where

$$S_{NX}^z \equiv \frac{1}{2} (|\mathcal{N}X\rangle\langle\mathcal{N}X| - |\mathcal{N}, 0\rangle\langle\mathcal{N}, 0|), \quad (53)$$

$$S_{NX}^x \equiv \frac{1}{2} (|\mathcal{N}X\rangle\langle\mathcal{N}, 0| + |\mathcal{N}, 0\rangle\langle\mathcal{N}X|), \quad (54)$$

are many-body pseudospin operators, and the Rabi frequencies Ω_{NX} are determined by

$$H_{\text{Rabi}} |\mathcal{N}, 0\rangle = \frac{1}{2} \Omega_0 \sum_\mu \mu \hat{c}_{\mu,e}^\dagger \hat{c}_{\mu,g} |\mathcal{N}, 0\rangle = \frac{1}{2} \Omega_{\mathcal{N},+} |\mathcal{N}, +\rangle + \frac{1}{2} \Omega_{\mathcal{N},-} |\mathcal{N}, -\rangle. \quad (55)$$

While the symmetric excited state $|\mathcal{N}, +\rangle$ is given in (48), at this point we have not explicitly solved for the asymmetric excited state $|\mathcal{N}, -\rangle$. The asymmetric state is implicitly defined by (55), and lies somewhere in the span of the $N - 1$ asymmetric states given in (49). Determining the symmetric-state Rabi frequency $\Omega_{\mathcal{N},+}$ is simply a matter of projecting the expression in (55) onto $|\mathcal{N}, +\rangle$, which yields

$$\Omega_{\mathcal{N},+} = \langle\mathcal{N}, +|\Omega_0 \sum_\mu \mu \hat{c}_{\mu,e}^\dagger \hat{c}_{\mu,g} |\mathcal{N}, 0\rangle = \Omega_0 \sum_{\mu \in \mathcal{N}} \frac{\mu}{\sqrt{N}} = \Omega_0 \sqrt{N} \bar{\mu}_{\mathcal{N}}, \quad (56)$$

where $\bar{\mu}_{\mathcal{N}} \equiv \sum_{\mu \in \mathcal{N}} \mu / N$ is the average nuclear spin $\mu \in \mathcal{N}$. In order to determine the asymmetric-state Rabi frequency $\Omega_{\mathcal{N},-}$, we rearrange (55) to find

$$\Omega_{\mathcal{N},-} |\mathcal{N}, -\rangle = \Omega_0 \sum_{\mu} \mu \hat{c}_{\mu,e}^{\dagger} \hat{c}_{\mu,g} |\mathcal{N}, 0\rangle - \Omega_{\mathcal{N},+} |\mathcal{N}, +\rangle = \Omega_0 \sum_{\mu \in \mathcal{N}} (\mu - \bar{\mu}_{\mathcal{N}}) \hat{c}_{\mu,e}^{\dagger} \hat{c}_{\mu,g} |\mathcal{N}, 0\rangle. \quad (57)$$

Denoting the standard deviation of nuclear spins $\mu \in \mathcal{N}$ by $\sigma_{\mathcal{N}}$, normalization of $|\mathcal{N}, -\rangle$ thus determines the asymmetric-state Rabi frequency

$$\Omega_{\mathcal{N},-} = \Omega_0 \left[\sum_{\mu \in \mathcal{N}} (\mu - \bar{\mu}_{\mathcal{N}})^2 \right]^{1/2} = \Omega_0 \sqrt{N} \sigma_{\mathcal{N}}, \quad (58)$$

which in turn implies that the asymmetric excited state $|\mathcal{N}, -\rangle$ is

$$|\mathcal{N}, -\rangle = \frac{1}{\sqrt{N}} \sum_{\mu \in \mathcal{N}} \left(\frac{\mu - \bar{\mu}_{\mathcal{N}}}{\sigma_{\mathcal{N}}} \right) \hat{c}_{\mu,e}^{\dagger} \hat{c}_{\mu,g} |\mathcal{N}, 0\rangle. \quad (59)$$

Figure 2 shows multiplicities of the magnitudes of reduced Rabi frequencies $\omega_{\mathcal{N}X} \equiv \Omega_{\mathcal{N}X} / \Omega_0 \sqrt{N}$ in a lattice with a uniform mixture of nuclear spins with $I = 9/2$ for single-site occupation numbers N which are achievable in current ^{87}Sr experiments [34]. On average, asymmetric-state Rabi frequencies are greater in magnitude, which becomes more pronounced for larger single-site occupation numbers.

B. Experimental signatures and comparison

We now consider samples of ^{87}Sr atoms in a uniform mixture of nuclear spins $\mu \in \{-I, -I + 1, \dots, I\}$ prepared in motional ground states of a rectangular lattice with depths $\mathcal{U} = (\mathcal{U}_x, \mathcal{U}_y, \mathcal{U}_z) = (41, 55, 69) E_{\text{R}}$, where $E_{\text{R}} \approx 3.5 \times 2\pi$ kHz is the lattice photon recoil energy of the atoms. Such samples can be prepared in experiments which can vary the single-site occupation number N , and which can control for the total number of atoms that are addressed by an external interrogation laser. Figure 3 shows the population of the excited 3P_0 orbital state when these atoms are interrogated for a time $t = \pi / \Omega_I$ by a laser with Rabi frequency $\Omega_I = 50 \times 2\pi$ Hz (i.e. for individual atoms with nuclear spin $\mu = I$) and detuning Δ from the single-atom $^1S_0 \rightarrow ^3P_0$ orbital excitation energy. The 3P_0 population peaks when the laser detuning Δ is equal to the many-body excitation energy $\Delta_{\mathcal{N}X} \equiv E_{\mathcal{N}X} - E_{\mathcal{N},0}$ for $X \in \{+, -\}$, as this is precisely when the on-resonance condition $\delta = 0$ is satisfied in the

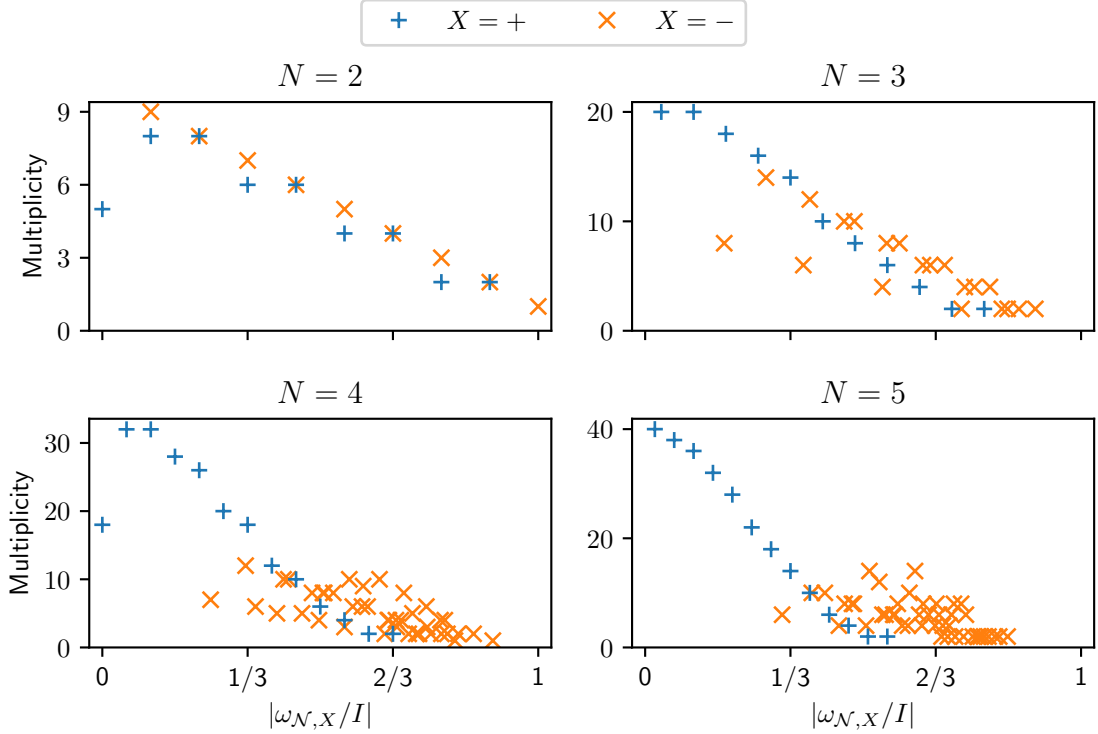


FIG. 2. Multiplicities of the magnitudes of reduced Rabi frequencies $\omega_{\mathcal{N}X} \equiv \Omega_{\mathcal{N}X}/\Omega_0\sqrt{N}$ in a lattice with a uniform mixture of nuclear spins with $I = 9/2$ and single-site occupation numbers N which are achievable in current ^{87}Sr experiments.

many-body Rabi Hamiltonian $H_{\mathcal{N}X}$ in (52). Due to experimental uncertainties which vary with single-site occupation number N , the heights of experimental peaks in figure 3 are not well-calibrated between different values of N . Nonetheless, figure 3 exhibits signatures of larger asymmetric-state Rabi frequencies than symmetric-state ones in the form of higher asymmetric-state peaks for fixed N .

Identifying peaks in excitation spectra such as in figure 3 constitutes a measurement of many-body excitation energies, which was performed in ref. [34] to detect signatures of effective multi-body interactions. Figure 4 shows a comparison between (i) experimental measurements of the many-body excitation energies $\Delta_{\mathcal{N}X}$ for all $(N, X) \in \{3, 4, 5\} \times \{+, -\}$ at various mean lattice depths \mathcal{U} , and (ii) the corresponding values of $\Delta_{\mathcal{N}X}$ predicted by the low-energy effective theory at different orders in the coupling constants. A known source of error in our effective theory comes from neglecting the inter-site matrix elements of all Hamiltonians. This error is discussed in Appendix E, and leads to theoretical uncertainties

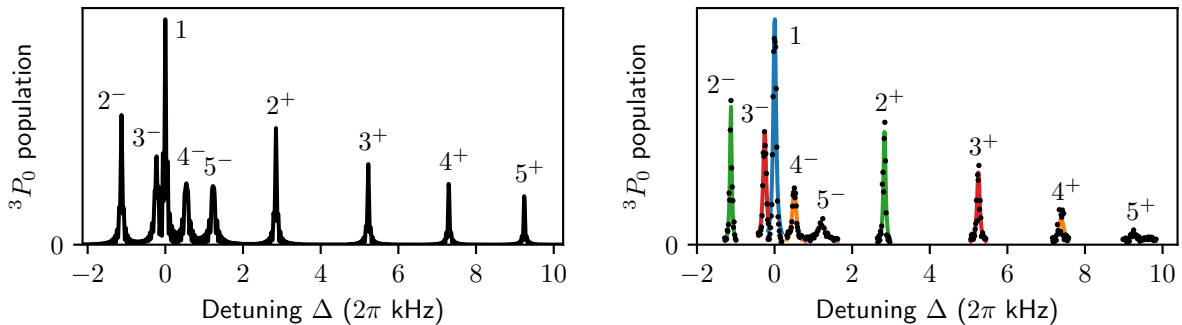


FIG. 3. Population (in arbitrary units) of the excited 3P_0 orbital state of ${}^{87}\text{Sr}$ atoms in a uniform mixture of nuclear spins. Atoms are prepared in the ground state of a lattice with depth $U = 54E_R$, where $E_R \approx 3.5 \times 2\pi$ kHz is the lattice photon recoil energy of the atoms, and interrogated by a laser with Rabi frequency $\Omega_I = 50 \times 2\pi$ Hz for a time $t = \pi/\Omega_I$. **(Left)** Populations predicted by the low-energy effective theory (with s -wave scattering parameters retrieved from ref. [19]), averaged over all nuclear spin combinations of $N \in \{1, \dots, 5\}$ atoms per lattice site for a fixed total atom number. **(Right)** Experimental measurements of 3P_0 populations retrieved from ref. [34], with Lorentzian fits to each peak as a visual guide. Resonance peaks are identified by the many-body orbital states which are excited at the peak.

represented by error bars on the $\mathcal{O}(G^3)$ theory in figure 4. A summary of figure 4 is provided in figure 5. We note that many-body interaction energy shifts are smaller for asymmetric ($-$) states than symmetric ($+$) ones due to the competition between contributions of opposite sign in the asymmetric case (see rows 2 and 3 of table I, where as a consequence of positive scattering lengths in the case of ${}^{87}\text{Sr}$, all U_{MX} for fixed M have the same sign). This competition is a many-body analogue of the two-body case with a competition between direct and exchange terms in the interaction energies of singly-excited states.

The results in figures 4 and 5 highlight a few important points about ultracold, high-density ${}^{87}\text{Sr}$ experiments and our low-energy effective theory. First, these experiments exhibit clear signatures of multi-body interactions, as evidenced by a stark disagreement between the observed many-body excitation energies Δ_{NX} and those that are predicted by the two-body $\mathcal{O}(G)$ theory. Multi-body interactions are thus crucial for understanding these high-density experiments in the context of a single-band Hubbard model, which naturally arises in the zero-temperature limit when all atoms occupy their motional ground state. Sec-

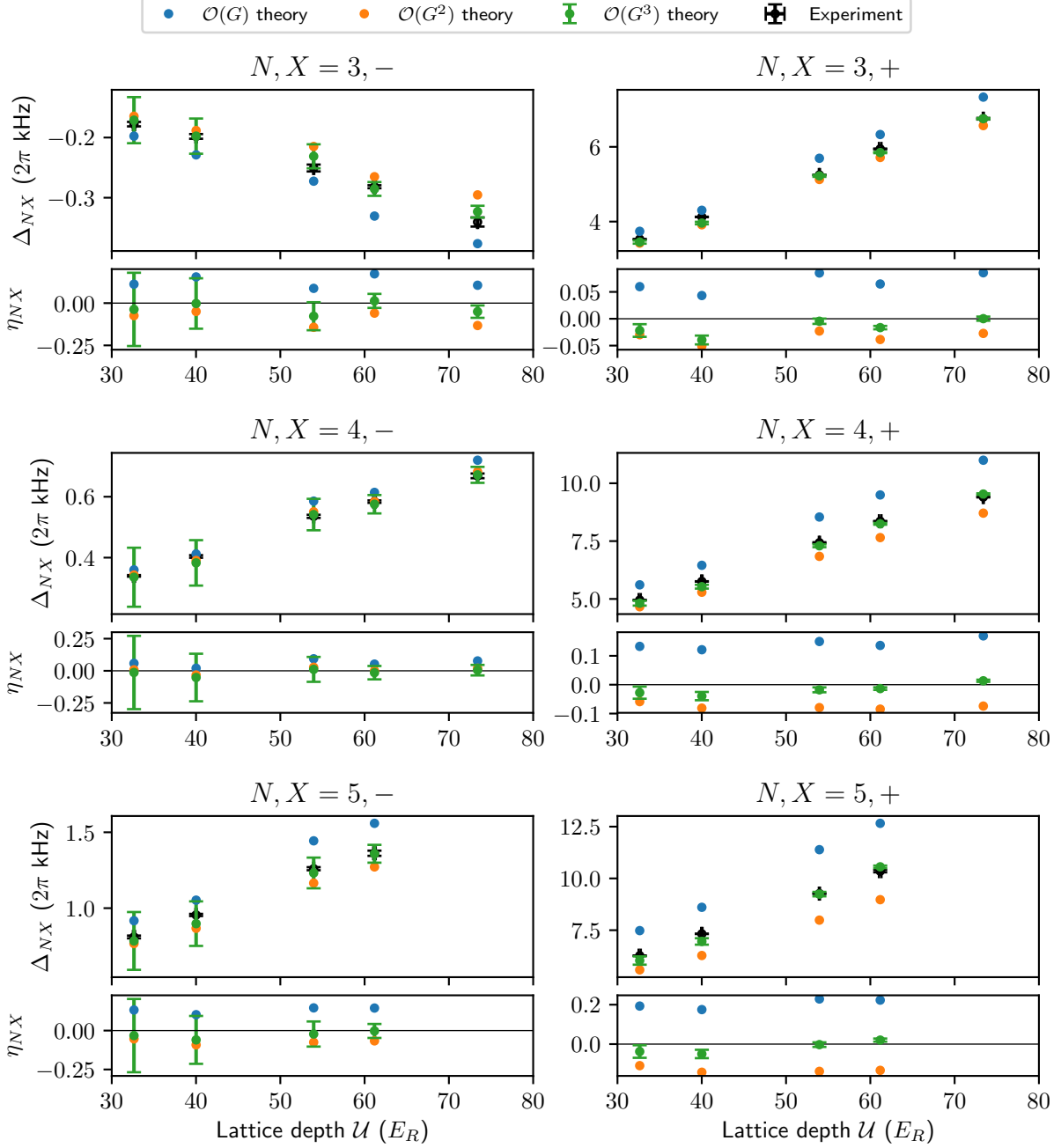


FIG. 4. Multi-body excitation energies of ultracold ^{87}Sr atoms at various lattice depths. The top plot in each sub-figure with fixed N, X shows the excitation energies $\Delta_{NX} \equiv E_{NX} - E_{N,0}$ measured experimentally in ref. [34] and those predicted by the low-energy effective theory at different orders in the coupling constants, when applicable both with and without four-body contributions. The bottom plot in each sub-figure shows the relative error $\eta_{NX} \equiv \Delta_{NX}^{\text{theory}} / \Delta_{NX}^{\text{experiment}} - 1$. Error bars represent experimental error or conservatively estimated theoretical uncertainties from nearest-neighbor hopping of virtual states in the low-energy effective theory (see Appendix E).

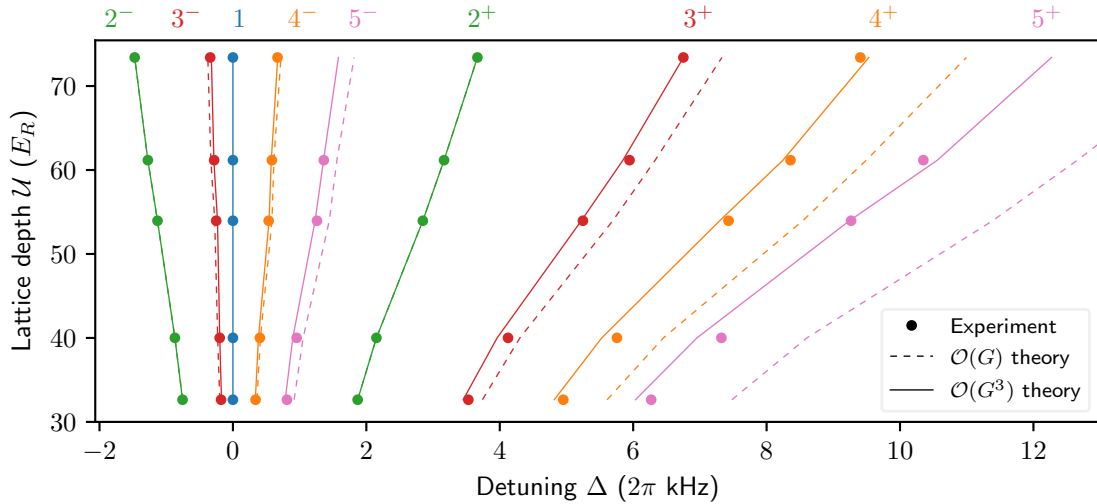


FIG. 5. Summary of the many-body excitation spectra in figure 4, retrieved from ref. [34].

ond, the inter-atomic interactions in these experiments are strong enough to require going beyond leading order for the description of multi-body interactions in the low-energy effective theory. The formally small quantities organizing our perturbation theory are two-body ground-state interaction energies (proportional to the couplings G_X) divided by the spectral gap of the single-atom Hamiltonian H_0 . These reduced (dimensionless) interaction energies vary from $\sim 0.05 - 0.15$ in the parameter regimes of the ^{87}Sr experiments considered here (see Appendix F). As experiments begin to operate at higher atom densities with amplified interaction effects, reliably predicting interaction energies may require going to yet higher orders in perturbation theory. Due to a combinatorial explosion of the number of diagrams which appear at increasing orders in the effective theory, however, we need more systematic methods to compute effective multi-body Hamiltonians at fourth order. In any case, we are agnostic as to whether such a calculation would provide better agreement between experiment and theory without first performing a detailed analysis of systematic errors.

C. Orbital-state dynamics of a nuclear spin mixture

In addition to spectral measurements of many-body interaction energies, we consider the dynamics of multiply-occupied lattice sites during spectroscopic interrogation. While these dynamics do not provide information about the nature or origin of effective multi-body

interactions, they provide tools and intuition for addressing the low-lying orbital excitations which are readily accessible in an experimental setting. If we initialize all atoms in the N -body ground state with an incoherent mixture of all nuclear spins, then we prepare the mixed state $\rho_{N,0} = \mathcal{P}_{N,0}/\text{tr } \mathcal{P}_{N,0}$, where

$$\mathcal{P}_{NX} \equiv \sum_{|\mathcal{N}|=N} |\mathcal{N}X\rangle\langle\mathcal{N}X| \quad (60)$$

is a projector onto the space of the N -body orbital states $|\mathcal{N}X\rangle$. Interrogating the atoms for a time t by a laser resonant with the excitation energy $\Delta_{N\pm}$ then gives us the state

$$\rho_N^{(\pm)}(t) = \frac{1}{\text{tr } \mathcal{P}_{N,0}} \sum_{|\mathcal{N}|=N} \exp(-it\Omega_{N\pm} S_{N\pm}^x) |\mathcal{N}, 0\rangle\langle\mathcal{N}, 0| \exp(it\Omega_{N\pm} S_{N\pm}^x), \quad (61)$$

where the Rabi frequencies $\Omega_{N,+}$, $\Omega_{N,-}$ and pseudo-spin operators $S_{N\pm}^x$ are respectively given in (56), (58), and (54). Denoting the eigenstates of $S_{N\pm}^x$ by

$$|\mathcal{N}, \mathcal{S}_{\pm}\rangle \equiv \frac{1}{\sqrt{2}} (|\mathcal{N}, 0\rangle + |\mathcal{N}\pm\rangle), \quad |\mathcal{N}, \mathcal{A}_{\pm}\rangle \equiv \frac{1}{\sqrt{2}} (|\mathcal{N}, 0\rangle - |\mathcal{N}\pm\rangle), \quad (62)$$

and defining the identity operator projected to the relevant subspace,

$$\mathbb{1}_{N\pm} \equiv |\mathcal{N}, 0\rangle\langle\mathcal{N}, 0| + |\mathcal{N}\pm\rangle\langle\mathcal{N}\pm| = |\mathcal{N}, \mathcal{S}_{\pm}\rangle\langle\mathcal{N}, \mathcal{S}_{\pm}| + |\mathcal{N}, \mathcal{A}_{\pm}\rangle\langle\mathcal{N}, \mathcal{A}_{\pm}|, \quad (63)$$

we can write the state $\rho_N^{(\pm)}(t)$ and excited-state projectors $\mathcal{P}_{N\pm}$ in the form

$$\rho_N^{(\pm)}(t) = \frac{1}{\text{tr } \mathcal{P}_{N,0}} \sum_{|\mathcal{N}|=N} \frac{1}{2} [\mathbb{1}_{N\pm} + e^{i2t\Omega_{N\pm}} |\mathcal{N}, \mathcal{S}_{\pm}\rangle\langle\mathcal{N}, \mathcal{A}_{\pm}| + e^{-i2t\Omega_{N\pm}} |\mathcal{N}, \mathcal{A}_{\pm}\rangle\langle\mathcal{N}, \mathcal{S}_{\pm}|], \quad (64)$$

and

$$\mathcal{P}_{N\pm} = \sum_{|\mathcal{N}|=N} \frac{1}{2} [\mathbb{1}_{N\pm} - |\mathcal{N}, \mathcal{S}_{\pm}\rangle\langle\mathcal{N}, \mathcal{A}_{\pm}| - |\mathcal{N}, \mathcal{A}_{\pm}\rangle\langle\mathcal{N}, \mathcal{S}_{\pm}|], \quad (65)$$

from which it follows that the net excited-state population at time t is

$$\langle\mathcal{P}_{N\pm}(t)\rangle \equiv \text{tr} [\rho_N^{(\pm)}(t) \mathcal{P}_{N\pm}] = \frac{1}{2} - \frac{1}{2} \langle\cos(2t\Omega_{N\pm})\rangle_{|\mathcal{N}|=N}, \quad (66)$$

where $\langle X \rangle_{|\mathcal{N}|=N} \equiv \sum_{|\mathcal{N}|=N} X / \text{tr } \mathcal{P}_{N,0}$ is an average of X over all choices of N distinct nuclear spins.

Figure 6 shows the excited-state population $\langle\mathcal{P}_{N\pm}(t)\rangle$ for several occupation numbers N . With the exception of $N = 2$, the asymmetric-state populations generally have an

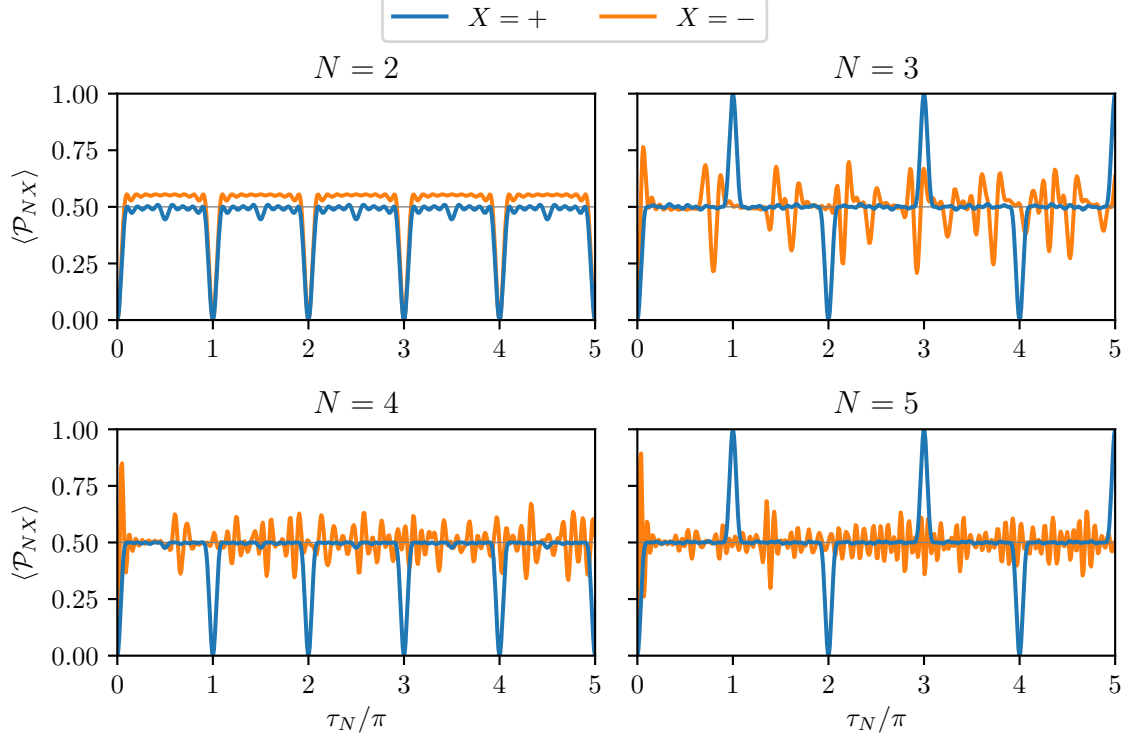


FIG. 6. Net population of the N -body orbital excited states $\{|\mathcal{N}\pm\rangle\}$ after interrogation of an initial mixed state $\rho_{N,0} = \mathcal{P}_{N,0}/\text{tr } \mathcal{P}_{N,0}$ for a reduced time $\tau_N \equiv t\Omega_0/\sqrt{N}$ (i.e. with real time t) by a laser with bare Rabi frequency Ω_0 which is resonant with the N -body excitation energy Δ_{NX} . Here \mathcal{P}_{NX} , defined in (60), is a projector onto the space of the N -body orbital states $|\mathcal{N}X\rangle$.

initial short period of growth before falling back to $\langle \mathcal{P}_{N,-} \rangle \approx 1/2$. This behavior can be understood by the fact that for fixed $N > 2$, any pair of Rabi frequencies $\Omega_{\mathcal{N}_1,-}, \Omega_{\mathcal{N}_2,-}$ with $\Omega_{\mathcal{N}_1,-} \neq \Omega_{\mathcal{N}_2,-}$ are mutually incommensurate, which implies that at times t with $\min_{|\mathcal{N}|=N} \{2t\Omega_{\mathcal{N},-}\} \gtrsim 1$ the averaging in (66) effectively becomes a pseudo-random sampling average of $\cos x$ over values of x , so $\langle \cos(2t\Omega_{\mathcal{N},-}) \rangle_{|\mathcal{N}|=N} \approx 0$. When $N = 2$, the asymmetric-state Rabi frequencies essentially take on the same values as the symmetric-state ones (see figure 2); the behavior of asymmetric-state population dynamics for $N = 2$ can therefore be understood by the following discussion of symmetric-state population dynamics.

To understand the periodic collapse and revival of symmetric-state populations in figure 6, we observe from (56) that the symmetric-state phases in (64) and (66) take the form

$$2t\Omega_{\mathcal{N},+} = \tau_N \sum_{\mu \in \mathcal{N}} 2\mu \quad \text{with} \quad \tau_N \equiv \frac{t\Omega_0}{\sqrt{N}}, \quad (67)$$

where for fermionic atoms with half-integer nuclear spin, 2μ is always an odd integer, which implies that the sum in (67) is an integer with the same parity (i.e. even/odd) as the occupation number N (i.e. the number of elements in \mathcal{N}). At reduced times $\tau_N = n\pi$ with integer n , therefore, if the occupation number N is even then all phases $2t\Omega_{\mathcal{N},+}$ are integer multiples of 2π , which leads to a collapse of the excited-state populations as $\rho_N^{(\pm)}(t)\Big|_{\tau_N=n\pi} = \rho_N^{(\pm)}(0) = \rho_{N,0}$. If the occupation N is odd, meanwhile, then the phases $2t\Omega_{\mathcal{N},+}$ are all odd (even) integer multiples of π for odd (even) n . This alignment of phases implies a complete population transfer to the excited state $\rho_{N,-} \equiv \mathcal{P}_{N,-}/\text{tr } \mathcal{P}_{N,-}$ for odd n , and a collapse back to the orbital ground state $\rho_{N,0}$ for even n , precisely as observed in figure 6.

V. SUMMARY AND OUTLOOK

Current 3-D optical lattice experiments with fermionic AEAs are capable of operating in the low-temperature, high-density, strongly-interacting limit where inter-atomic interactions set the dominant energy scale governing system dynamics. For AEAs with total nuclear spin I and $N = 2I + 1$ nuclear spin states, these interactions exhibit an exotic $\text{SU}(N)$ symmetry which is of great interest for near-term quantum simulations of $\text{SU}(N)$ spin models and lattice field theories. Working in the deep-lattice limit and the experimental regime of at most one atom occupying each nuclear spin state on any lattice site, we have derived a low-energy effective theory of these atoms. Our theory exhibits emergent multi-body interactions that inherit the $\text{SU}(N)$ symmetry of the bare two-body interactions. Considering a restriction of our theory to the subspace of at most one orbital excitation per lattice site, we found that the $\text{SU}(N)$ symmetry of all M -body Hamiltonians allowed us to express them in a simple form, and to fully characterize their eigenstates and spectra. Capitalizing on the extreme precision of state-of-the-art clock spectroscopy, we have tested spectral predictions of our theory against direct experimental measurements of the many-body ^{87}Sr excitation spectrum. This comparison shows good agreement between theory and experiment, clearly demonstrating the need to consider multi-body effects for understanding the low-energy physics of high density AEA samples on a 3-D lattice. Finally, we analyzed the many-body orbital-state dynamics of multiply-occupied lattice sites prepared in a nuclear spin mixture and interrogated via Rabi spectroscopy. This analysis is useful for future experimental probes of many-body state structures, as well as for the preparation of long-lived states

with multi-partite entanglement (i.e. $|\mathcal{N}\pm\rangle$) which may be used as a resource to perform quantum information processing tasks.

Despite the nominal success of our low-energy effective theory in reproducing experimental observations, there remains room for improvement in the form of controlled, systematic treatment of higher-order and tunneling processes. Nonetheless, our work makes a major step towards the experimental investigation of multi-body $SU(N)$ physics, providing the necessary framework for future studies going beyond the deep-lattice limit to realize multi-body super-exchange dynamics and orbital $SU(N)$ quantum magnetism with AEs.

ACKNOWLEDGEMENTS

We acknowledge helpful discussions with R. B. Hutson, G. E. Marti, S. L. Campbell, J. Ye, P. Julienne, J. P. D’Incao, C. Kennedy, and L. Radzihovsky; and in particular close correspondence and technical contributions from A. Goban. This work is supported by the Air Force Office of Scientific Research (AFOSR) grant FA9550-18-1-0319; the AFOSR Multidisciplinary University Research Initiative (MURI) grant; the Defense Advanced Research Projects Agency (DARPA) and Army Research Office (ARO) grant W911NF-16-1-0576; the National Science Foundation (NSF) grant PHY-1820885; JILA-NSF grant PFC-173400; and the National Institute of Standards and Technology (NIST).

APPENDICES

Appendix A: Derivation of the effective Hamiltonian expansion

Suppose we have a Hamiltonian H_0 on a Hilbert space $\mathcal{H} = \mathcal{G}_0 \oplus \mathcal{E}_0$ for a zero-energy manifold \mathcal{G}_0 decoupled from a positive-energy manifold \mathcal{E}_0 , and that we perturb H_0 by an operator V which weakly couples \mathcal{G}_0 and \mathcal{E}_0 . For all $|\psi_g\rangle \in \mathcal{G}_0$ and $|\phi_e\rangle, |\chi_e\rangle \in \mathcal{E}_0$, we have $\langle\psi_g|H_0|\psi_g\rangle = 0$, $\langle\phi_e|H_0|\psi_g\rangle = 0$, and $|\langle\phi_e|V|\psi_g\rangle| \ll \langle\chi_e|H_0|\chi_e\rangle$. The net Hamiltonian $H = H_0 + V$ will naturally admit a decomposition of the Hilbert space as $\mathcal{H} = \mathcal{G} \oplus \mathcal{E}$ for a subspace \mathcal{G} which is spanned by the low-energy eigenstates of H and has the same dimension as \mathcal{G}_0 , i.e. $|\mathcal{G}| = |\mathcal{G}_0|$.

We can perform a canonical transformation between \mathcal{G} and \mathcal{G}_0 which yields an *effective Hamiltonian* H_{eff} on \mathcal{G}_0 that reproduces the spectrum of H on \mathcal{G} [49]. Given an eigenbasis

$\{|\alpha_0\rangle\}$ for H_0 on \mathcal{G}_0 and $\{|\alpha\rangle\}$ for H on \mathcal{G} , this transformation is implemented by a unitary U for which $|\alpha_0\rangle = U|\alpha\rangle$ and $U \rightarrow \mathbb{1}$ as $\|V\| \rightarrow 0$. The effective Hamiltonian is then simply

$$H_{\text{eff}} = UHU^\dagger. \quad (\text{A1})$$

The prescription in (A1) for constructing an effective Hamiltonian is commonly known as a Schieffer-Wolff transformation [50]. Unitaries U which follow this prescription are not unique, and different choices of U amount to different realizations of the Schieffer-Wolff transformation. In ref. [49], the authors construct the unique operator S which generates a *direct* or *minimal* rotation $U_{\text{min}} = e^S$ between \mathcal{G} and \mathcal{G}_0 , and use this construction to expand (A1) as a perturbative series in V . The rotation U_{min} is minimal in the sense that it minimizes the distance of candidate unitaries U from the identity $\mathbb{1}$ with respect to the Euclidian operator norm¹ $\|X\|_{\text{E}} \equiv \sqrt{\text{tr}(X^\dagger X)}$. This rotation is determined uniquely by enforcing (i) that the generator S is strictly block-off-diagonal with respect to \mathcal{G}_0 and \mathcal{E}_0 , (ii) that the norm $\|S\|_{\text{E}} < \pi/2$, and (iii) that the block-off-diagonal parts of (A1) are zero.

To summarize the solution in ref. [49], the effective Hamiltonian H_{eff} induced by a direct rotation can be expanded as

$$H_{\text{eff}} = \sum_{p \geq 0} H_{\text{eff}}^{(p)}, \quad (\text{A2})$$

where $H_{\text{eff}}^{(p)}$ is order p in V . Letting \mathcal{P}_0 denote the projector onto \mathcal{G}_0 , $\mathcal{Q}_0 \equiv \mathbb{1} - \mathcal{P}_0$ denote the projector onto \mathcal{E}_0 , and X denote any operator on \mathcal{H} , we define the superoperators

$$\mathcal{D}X \equiv \mathcal{P}_0 X \mathcal{P}_0 + \mathcal{Q}_0 X \mathcal{Q}_0, \quad \mathcal{O}X \equiv \mathcal{P}_0 X \mathcal{Q}_0 + \mathcal{Q}_0 X \mathcal{P}_0, \quad (\text{A3})$$

which select out the diagonal (\mathcal{D}) and off-diagonal (\mathcal{O}) parts of X with respect to \mathcal{G}_0 and \mathcal{E}_0 , and

$$\mathcal{L}X \equiv \sum_{\alpha, \beta} \frac{|\alpha\rangle\langle\alpha| \mathcal{O}X |\beta\rangle\langle\beta|}{E_\alpha - E_\beta} \quad \text{where} \quad H_0 = \sum_{\alpha} E_\alpha |\alpha\rangle\langle\alpha|. \quad (\text{A4})$$

The first few terms of the expansion in (A2) are then, as derived in ref. [49],

$$H_{\text{eff}}^{(0)} = \mathcal{P}_0 H_0 \mathcal{P}_0, \quad H_{\text{eff}}^{(1)} = \mathcal{P}_0 V \mathcal{P}_0, \quad (\text{A5})$$

¹ The Euclidean operator norm is also known as the $L_{2,2}$, Hilbert-Schmidt, or Frobenius norm.

$$H_{\text{eff}}^{(2)} = -\frac{1}{2}\mathcal{P}_0 [\mathcal{O}V, \mathcal{L}V] \mathcal{P}_0, \quad H_{\text{eff}}^{(3)} = \frac{1}{2}\mathcal{P}_0 [\mathcal{O}V, \mathcal{L} [\mathcal{D}V, \mathcal{L}V]] \mathcal{P}_0. \quad (\text{A6})$$

Exploiting the fact that in our case $\langle \psi | H_0 | \psi \rangle = 0$ for all $|\psi\rangle \in \mathcal{G}_0$, we let $\mathcal{B}_0(\mathcal{E}_0)$ denote an eigenbasis of H_0 for \mathcal{E}_0 and define the operator

$$\mathcal{I} \equiv \sum_{|\alpha\rangle \in \mathcal{B}_0(\mathcal{E}_0)} \frac{|\alpha\rangle\langle\alpha|}{E_\alpha}, \quad (\text{A7})$$

which sums over projections onto excited states with corresponding energetic suppression factors. We then expand

$$\mathcal{L}X = \mathcal{O}(\mathcal{L}X) = \mathcal{Q}_0\mathcal{L}X\mathcal{P}_0 + \mathcal{P}_0\mathcal{L}X\mathcal{Q}_0 = \mathcal{I}X\mathcal{P}_0 - \mathcal{P}_0X\mathcal{I}, \quad (\text{A8})$$

which simplifies the expression for $H_{\text{eff}}^{(2)}$ as

$$H_{\text{eff}}^{(2)} = -\frac{1}{2}\mathcal{P}_0 ([\mathcal{O}V, \mathcal{I}V\mathcal{P}_0] - [\mathcal{O}V, \mathcal{P}_0V\mathcal{I}]) \mathcal{P}_0 = -\mathcal{P}_0V\mathcal{I}V\mathcal{P}_0. \quad (\text{A9})$$

Working toward a similar expansion for $H_{\text{eff}}^{(3)}$, we compute

$$[\mathcal{D}V, \mathcal{L}V] = [\mathcal{D}V, \mathcal{I}V\mathcal{P}_0] - [\mathcal{D}V, \mathcal{P}_0V\mathcal{I}] = \mathcal{O}(V\mathcal{I}V) - \mathcal{I}V\mathcal{P}_0V\mathcal{P}_0 - \mathcal{P}_0V\mathcal{P}_0V\mathcal{I}, \quad (\text{A10})$$

and in turn

$$H_{\text{eff}}^{(3)} = \frac{1}{2}\mathcal{P}_0 ([\mathcal{O}V, \mathcal{I} [\mathcal{D}V, \mathcal{L}V] \mathcal{P}_0] - [\mathcal{O}V, \mathcal{P}_0 [\mathcal{D}V, \mathcal{L}V] \mathcal{I}]) \mathcal{P}_0 \quad (\text{A11})$$

$$= \frac{1}{2}\mathcal{P}_0 (V\mathcal{I} [\mathcal{D}V, \mathcal{L}V] + [\mathcal{D}V, \mathcal{L}V] \mathcal{I}V) \mathcal{P}_0 \quad (\text{A12})$$

$$= \mathcal{P}_0V\mathcal{I}V\mathcal{I}V\mathcal{P}_0 - \frac{1}{2}\mathcal{P}_0V\mathcal{I}^2V\mathcal{P}_0V\mathcal{P}_0 - \frac{1}{2}\mathcal{P}_0V\mathcal{P}_0V\mathcal{I}^2V\mathcal{P}_0 \quad (\text{A13})$$

$$= \mathcal{P}_0V\mathcal{I}V\mathcal{I}V\mathcal{P}_0 - \frac{1}{2}[\mathcal{P}_0V\mathcal{P}_0, \mathcal{P}_0V\mathcal{I}^2V\mathcal{P}_0]_+, \quad (\text{A14})$$

where $[X, Y]_+ \equiv XY + YX$. The expressions in (A5), (A9), and (A14) complete the derivation for our expansion of the effective interaction Hamiltonian $H_{\text{int}}^{\text{eff}}$ in (11) through third order. In the case of ultracold atoms on a lattice, the motional ground-state subspace \mathcal{G}_0 actually contains many internal atomic states with different energies. Nonetheless, the total Hilbert space is completely separable into uncoupled subspaces associated with each symmetrized many-body internal atomic state. One can therefore diagonalize the interaction Hamiltonian with respect to these internal states and derive an effective theory within each of the corresponding subspaces, in each case setting the appropriate ground-state energy to zero. This procedure is equivalent to simultaneously calculating the effective Hamiltonian $H_{\text{int}}^{\text{eff}}$ for all internal states via the prescriptions we have provided, but letting E_α denote only the motional excitation energy of states $|\alpha_0\rangle \in \mathcal{B}_0(\mathcal{E}_0)$.

Appendix B: Diagram counting and symmetry factors

The fact that we include factors of $1/2$ from the bare two-body interaction Hamiltonian H_{int} in the definition of diagrams implies that p -vertex diagrams acquire a factor of $1/2^p$. In practice, however, these factors are exactly cancelled out by corresponding symmetry factors in all M -body diagrams with $M > 2$. As an illustrative example, consider the second-order effective Hamiltonian $H_{\text{int}}^{(2)}$ in (13), which expanded in full reads

$$H_{\text{int}}^{(2)} = - \sum_{m+n>0} \mathcal{P}_0 \left(\frac{1}{2} K_{mn} G_{s't'}^{st} \hat{c}_{\rho s'}^\dagger \hat{c}_{\sigma t'}^\dagger \hat{c}_{n\sigma t} \hat{c}_{m\rho s} \right) \frac{1}{E_{mn}} \left(\frac{1}{2} K_{mn} G_{q'r'}^{qr} \hat{c}_{m\mu q'}^\dagger \hat{c}_{n\nu r'}^\dagger \hat{c}_{\nu r} \hat{c}_{\mu q} \right) \mathcal{P}_0. \quad (\text{B1})$$

The three-body terms in this Hamiltonian have $|\{\mu, \nu, \rho, \sigma\}| = 3$ and only one virtually excited atom. The non-vanishing three-body terms must therefore either have $\rho \in \{\mu, \nu\}$ and contain a factor of the form $\hat{c}_X^\dagger \hat{c}_{\sigma t'}^\dagger \hat{c}_{\sigma t} \hat{c}_Y$, or have $\sigma \in \{\mu, \nu\}$ with a factor of the form $\hat{c}_{\rho s'}^\dagger \hat{c}_X^\dagger \hat{c}_Y \hat{c}_{\rho s}$, where the labels X, Y both address whichever nuclear spin (i.e. μ or ν) was excited in the corresponding term. Diagrammatically, we have terms of the form

$$\begin{array}{ccc} \begin{array}{c} \mu q \\ \nu r \end{array} & \begin{array}{c} Z \\ Y \\ X \end{array} & \begin{array}{c} \sigma t \\ \sigma t' \end{array} & \text{and} & \begin{array}{c} \mu q \\ \nu r \end{array} & \begin{array}{c} Z \\ Y \\ X \end{array} & \begin{array}{c} \rho s \\ \rho s' \end{array} & . \end{array} \quad (\text{B2})$$

Observing that $\hat{c}_{\rho s'}^\dagger \hat{c}_X^\dagger \hat{c}_Y \hat{c}_{\rho s} = \hat{c}_X^\dagger \hat{c}_{\rho s'}^\dagger \hat{c}_{\rho s} \hat{c}_Y$, however, it is clear that both of the terms represented in (B2) are equal up to the re-indexing $(\sigma, t, t') \leftrightarrow (\rho, s, s')$. There is therefore a symmetry factor of 2 associated with the second vertex of the diagrams in (B2), which cancels out with the explicit factor of $1/2$ at that vertex, i.e. the first factor of $1/2$ in (B1). A symmetry factor of essentially identical origin appears at every vertex with an “incoming” virtual state, as in e.g. the second and third vertices of

$$\begin{array}{ccc} \begin{array}{c} \mu q \\ \nu r \end{array} & \begin{array}{c} Z \\ Y \\ X \end{array} & \begin{array}{c} \sigma t \\ \sigma t' \end{array} & \text{and} & \begin{array}{c} \mu q \\ \nu r \end{array} & \begin{array}{c} Z \\ Y \\ X \end{array} & \begin{array}{c} \rho s \\ \rho s' \end{array} & . \end{array} \quad (\text{B3})$$

or the last vertex of

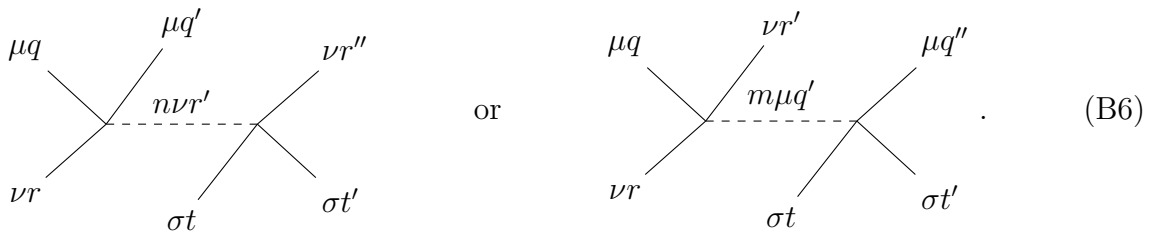
$$\begin{array}{ccc} \begin{array}{c} \mu q \\ \nu r \end{array} & \begin{array}{c} Z \\ Y \\ X \end{array} & \begin{array}{c} \sigma t \\ \sigma t' \end{array} & . \end{array} \quad (\text{B4})$$

We can thus account for cancellations of $1/2$ at all vertices except those which address two “initial” ground-state atoms, as in the first vertex of the diagrams in (B2) and (B3), or the first two vertices of the diagram in (B4). For such vertices, there are two possibilities: either

- (i) both edges leaving the vertex in question (i.e. leaving to the right) terminate at different vertices, as in the examples above, or
- (ii) both edges leaving the vertex in question terminate at the same vertex, as in for example the first vertex of



In the former case, (i), the vertex in question has an associated symmetry factor of 2 to account for the possibility of a nuclear spin exchange at that vertex. Considering again our example of the second-order effective Hamiltonian $H_{\text{int}}^{(2)}$ in (B1), the non-vanishing three-body terms must either have $m = 0$ and contain the factor $\hat{c}_{\mu q}^\dagger \hat{c}_{n\nu r'}^\dagger \hat{c}_{\nu r} \hat{c}_{\mu q}$, or have $n = 0$ with the factor $\hat{c}_{m\mu q}^\dagger \hat{c}_{\nu r'}^\dagger \hat{c}_{\nu r} \hat{c}_{\mu q}$, which diagrammatically translates to



These terms are equal up to the re-indexing $(\nu, r, r', r'', n) \leftrightarrow (\mu, q, q', q'', m)$, which implies that there is a symmetry factor of 2 associated with the first vertex of the diagrams in (B6). A symmetry factor of identical origin is associated with the first vertex of the diagrams in (B3), and the first two vertices of the diagram in (B4).

The final case we must consider is (ii), which occurs in the first vertex of (B5). In this case, the symmetry factor of 2 which appears in case (i) to account for the possibility of a nuclear spin exchange simply gets “pushed forward” to the vertex at which the two nuclear

spins in question part ways, e.g. to account for the two possibilities

$$\text{and} \quad (B7)$$

which are equal up to the re-indexing $(\nu, s, s', s'', s''', m) \leftrightarrow (\mu, r, r', r'', r''', \ell)$. The arguments for a symmetry factor in cases (i) and (ii) fail only if the two nuclear spins in question take identical paths through the internal vertices of a diagram, such that there is no meaningful sense in which two diagrams can be said to differ by a nuclear spin exchange, as in (B6) and (B7). If two atoms take identical paths through the internal vertices of a diagram, however, then they have only participated in a two-body process, as in

$$\dots \quad (B8)$$

After summing over all free indices, therefore, all two-body diagrams have a remaining factor of $1/2$ from the first vertex. In all connected M -body diagrams with $M > 2$, meanwhile, every factor of $1/2$ can be identified one-to-one with a corresponding symmetry factor of 2.

Appendix C: Effective coupling constants in a lattice

Due to our choice of renormalization scheme in section III B, the interaction energies prescribed by our low-energy effective theory for multiply-occupied lattice sites are not given directly by the coupling constants G_X defined by the free-space scattering lengths a_X in (3). Instead, we must first compute effective coupling constants $G_X^{\text{lattice}}(\mathcal{U})$ in a lattice with depth \mathcal{U} , and in turn use the effective coupling constants to compute interaction energies. As the renormalization procedure $G_X \rightarrow G_X^{\text{lattice}}$ is identical for all coupling constants, we henceforth drop the subscript $X \in \{\text{gg}, \text{eg}^-, \text{eg}^+, \text{ee}\}$ on coupling constants G_X in the remainder of this Appendix. To further simplify notation, we will also neglect the explicit dependence of parameters on the lattice depth \mathcal{U} , which we generally keep fixed.

Proper calculations of the interaction energy of two ultracold fermions in an optical lattice were performed in refs. [43] and [57] using a two-channel model of a Feshbach resonance, yielding prescriptions for computing effective coupling constants in a lattice from free-space

interaction parameters. These calculations, however, are both analytically and numerically involved. We therefore instead opt to use a modified version of the considerably simpler single-channel calculation in ref. [44] of the interaction energy of two ultracold atoms in a harmonic trap. Our approach is equivalent to the calculation of Hubbard parameters performed in ref. [58], and has been demonstrated to reproduce correct results in the limit of a deep lattice (compared to the lattice photon recoil energy) and small positive scattering lengths (compared to the effective harmonic oscillator length) [57].

The exact result in Eq. 16 of ref. [44] for the interaction energy of two ultracold atoms in a harmonic oscillator with angular trap frequency ω can be written in the form

$$(G_{\text{free}}K_{\text{HO}}/\omega)^{-1} = \frac{\sqrt{\pi} \Gamma(-G_{\text{HO}}K_{\text{HO}}/2\omega)}{\Gamma(-G_{\text{HO}}K_{\text{HO}}/2\omega - 1/2)}, \quad K_{\text{HO}} \equiv \int d^3x |\phi_0^{\text{HO}}|^4, \quad (\text{C1})$$

where G_{HO} is an effective coupling constant in the harmonic trap, $\phi_0^{\text{HO}}(x)$ is the corresponding non-interacting ground-state wavefunction, and Γ is the gamma function. The expression in (C1) can be solved numerically as is, or expanded about $G_{\text{HO}}K_{\text{HO}}/\omega = 0$ to get

$$G_{\text{free}}^{-1} = G_{\text{HO}}^{-1} \sum_{n=0}^{\infty} c_n (G_{\text{HO}}K_{\text{HO}}/\omega)^n, \quad (\text{C2})$$

where the first few coefficients are

$$c_0 = 1, \quad c_1 = 1 - \ln 2, \quad c_2 = -\frac{\pi^2}{24} - \ln 2 + \frac{1}{2} (\ln 2)^2. \quad (\text{C3})$$

The series in (C2) can in turn be inverted to solve for G_{HO} with an expansion of the form

$$G_{\text{HO}} = G_{\text{free}} \sum_{n=0}^{\infty} \tilde{c}_n (G_{\text{free}}K_{\text{HO}}/\omega)^n, \quad (\text{C4})$$

where if we truncate the series in (C2) at $n = 2$, the first few coefficients of (C4) are

$$\tilde{c}_0 = 1, \quad \tilde{c}_1 = 1 - \ln 2, \quad \tilde{c}_2 = -\frac{\pi^2}{24} - \ln 2 + \frac{1}{2} (\ln 2)^2 + (1 - \ln 2)^2. \quad (\text{C5})$$

The coefficients \tilde{c}_n thus found are consistent with the coefficients $c_2^{(n+1)}$ reported in table 1 of ref. [35], in which the authors compute the first few terms of the two-body Hamiltonian H_2 directly as expressed in (15) by using a renormalization scheme which subtracts off divergences term by term.

All of the above results are exact for two atoms in a harmonic oscillator interacting via s -wave scattering. In order to adapt these results for a lattice, we expand the lattice potential about a lattice site centered at $x = (0, 0, 0)$ as

$$\mathcal{U} \sin^2(k_L \cdot x) \approx \mathcal{U} \left[(k_L^x k_L^y k_L^z)^{1/3} x \right]^2 = \frac{1}{2} m_A \omega_{\text{eff}}^2 x^2, \quad \omega_{\text{eff}} \equiv \sqrt{2 \mathcal{U} k_L^2 / m_A}, \quad (\text{C6})$$

where $k_L = (k_L^x, k_L^y, k_L^z)$ is the lattice wavenumber, m_A is the atomic mass, and ω_{eff} is an effective angular harmonic trap frequency. We then use ω_{eff} in place of ω in (C1), and use an overlap integral K computed with the ground-state wavefunctions ϕ_0 in a lattice rather than those in a harmonic oscillator. We retrieve free-space s -wave scattering lengths a_{free} for ^{87}Sr from ref. [19] to determine the free-space coupling constants $G_{\text{free}} \equiv (4\pi/m_A) a_{\text{free}}$. This procedure yields an effective coupling constant G_{lattice} given by

$$(G_{\text{free}} K / \omega_{\text{eff}})^{-1} = \frac{\sqrt{\pi} \Gamma(-G_{\text{lattice}} K / 2\omega_{\text{eff}})}{\Gamma(-G_{\text{lattice}} K / 2\omega_{\text{eff}} - 1/2)}, \quad (\text{C7})$$

with a solution

$$G_{\text{lattice}} = G_{\text{free}} \sum_{n=0}^{\infty} \tilde{c}_n (G_{\text{free}} K / \omega_{\text{eff}})^n, \quad (\text{C8})$$

where the first few coefficients are provided in (C5).

Appendix D: Momentum-dependent s -wave interactions

In addition to the renormalization of coupling constants discussed in Appendix C, computing two-body interaction energies $E_{NX}^{(2)}$ at third order in the low-energy effective theory requires accounting for the contribution of momentum-dependent s -wave interactions. At next-to-leading order in the relative momentum k between two atoms, the effective momentum-dependent scattering length a_{eff} is given in terms of the zero-momentum scattering length a by [45–47]

$$\frac{1}{a_{\text{eff}}} = \frac{1}{a} - \frac{1}{2} r_{\text{eff}} k^2 = \frac{1}{a} \left(1 - \frac{1}{2} r_{\text{eff}} a k^2 \right), \quad (\text{D1})$$

which for $r_{\text{eff}} a k^2 \ll 1$, implies that

$$a_{\text{eff}} \approx a \left(1 + \frac{1}{2} r_{\text{eff}} a k^2 \right) = a + \frac{1}{2} r_{\text{eff}} a^2 k^2. \quad (\text{D2})$$

Here r_{eff} is an effective range of $\mathcal{O}(k^2)$ interactions, determined in atomic units by the scattering length a and van der Waals C_6 coefficient by [47]

$$r_{\text{eff}} = \frac{1}{3}\xi^{-2}\chi(1 - 2\chi + 2\chi^2)a, \quad \text{where} \quad \xi \equiv \frac{\Gamma(3/4)}{\Gamma(1/4)}, \quad \chi \equiv \sqrt{2}\xi \frac{(m_{\text{A}}C_6)^{1/4}}{a}, \quad (\text{D3})$$

and Γ is the gamma function. As $\chi \sim 1$ for ^{87}Sr , the momentum-dependent correction to the effective scattering length a_{eff} is $\mathcal{O}(a^3)$ without an additional separation of scales (i.e. which could have occurred if we had $\chi \ll 1$ or $\chi \gg 1$). The momentum-independent $\mathcal{O}(k^0)$ contribution to a_{eff} in (D2) gives rise to the bare two-body interactions in (7) by use of an unregularized contact (i.e. δ -function) potential, while the momentum-dependent $\mathcal{O}(k^2)$ term gives rise to the interaction Hamiltonian [35, 46]

$$H'_{\text{int}} \equiv \frac{1}{2} \sum G'^{qr}_{st} \int d^3x d^3y \delta(z) \left[\hat{\psi}_{\mu q}^\dagger(x) \hat{\psi}_{\nu r}^\dagger(y) \right] \hat{k}_z^2 \left[\hat{\psi}_{\nu t}(y) \hat{\psi}_{\mu s}(x) \right], \quad (\text{D4})$$

where

$$z \equiv x - y, \quad \hat{k}_z^2 \equiv -\frac{1}{2} \left(\vec{\nabla}_z^2 + \overleftarrow{\nabla}_z^2 \right), \quad (\text{D5})$$

and the primed couplings G'^{qr}_{st} are defined similarly to unprimed couplings G^{qr}_{st} in (3) and (4), but with scattering lengths $a \rightarrow r_{\text{eff}}a^2/2$ and the effective range r_{eff} defined by (D3) for each scattering length with an appropriate C_6 coefficient. We retrieve C_6 coefficients for ^{87}Sr from the supplementary material of ref. [19]. The squared relative momentum operator k_z^2 is represented by symmetrized left- and right-acting derivative operators in order to preserve manifest Hermiticity of H'_{int} . At third order in the low-energy effective theory developed in section III, the bare momentum-dependent interactions in (17) yield only the effective two-body Hamiltonian

$$H'_2 \equiv \frac{1}{2} K' \sum G'^{qr}_{st} \hat{c}_{\mu s}^\dagger \hat{c}_{\nu t}^\dagger \hat{c}_{\nu r} \hat{c}_{\mu q}, \quad (\text{D6})$$

where, letting $\text{Re}[X]$ denote the real part of X ,

$$K' \equiv \frac{1}{2} \int d^3x \text{Re} \left[(\phi_0^*)^2 \left(\vec{\nabla} \phi_0 \cdot \overleftarrow{\nabla} \phi_0 - \phi_0 \overrightarrow{\nabla}^2 \phi_0 \right) \right]. \quad (\text{D7})$$

Appendix E: Bounds on theoretical uncertainties from inter-site effects

In our overview of the relevant one- and two-particle physics of ultracold atoms on a lattice (section II), we made two approximations which introduce error into the low-energy

effective theory. Both approximations concern the on-site locality of the single- and two-body Hamiltonians: we assumed that (i) tunneling between lattice sites and (ii) inter-site interactions are negligible. These approximations are justified for single-particle motional ground states of atoms in a deep lattice, but generally break down when considering virtual states occupying highly excited motional levels, whose spatial wavefunctions can span multiple lattice sites. Nonetheless, we can place upper bounds on the magnitude of inter-site corrections to the effective on-site interaction Hamiltonians by treating tunneling and inter-site interactions of virtual excited states perturbatively and assuming no energetic penalty for nearest-neighbor hopping. These bounds can be used to diagnose the breakdown of the on-site effective theory, and signal when a more careful consideration of inter-site effects is necessary to make precise predictions about many-body spectra and dynamics.

If we still assume negligible overlap between single-particle ground-state wavefunctions in different lattice sites but consider nearest-neighbor wavefunction overlaps of states with motional excitations, our one-body and bare two-body Hamiltonians become

$$H_0 = \sum E_n \hat{c}_{in\mu s}^\dagger \hat{c}_{in\mu s} - \sum_{\substack{\langle i,j \rangle \\ m,n>0}} \left(t_{mn} \hat{c}_{jn\mu s}^\dagger \hat{c}_{im\mu s} + \text{h.c.} \right), \quad (\text{E1})$$

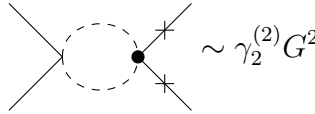
and

$$\begin{aligned} H_{\text{int}} = & \frac{1}{2} \sum K_{mn}^{kl} G_{st}^{qr} \hat{c}_{im\mu s}^\dagger \hat{c}_{in\nu t}^\dagger \hat{c}_{il\nu r} \hat{c}_{ik\mu q} + \frac{1}{2} \sum_{\substack{\langle i,j \rangle \\ n>0}} G_{\rho s; \sigma t}^{\mu q; \nu r} \left(\mathcal{K}_n \hat{c}_{j,0,\rho s}^\dagger \hat{c}_{j,0,\sigma t}^\dagger \hat{c}_{j,0,\nu r} \hat{c}_{in\mu q} + \text{h.c.} \right) \\ & + \frac{1}{2} \sum_{\substack{\langle i,j \rangle \\ m,n>0}} G_{\rho s; \sigma t}^{\mu q; \nu r} \left(\mathcal{K}_{mn} \hat{c}_{j,0,\rho s}^\dagger \hat{c}_{j,0,\sigma t}^\dagger \hat{c}_{in\nu r} \hat{c}_{im\mu q} + \tilde{\mathcal{K}}_{mn} \hat{c}_{in\rho s}^\dagger \hat{c}_{j,0,\sigma t}^\dagger \hat{c}_{j,0,\nu r} \hat{c}_{im\mu q} + \text{h.c.} \right), \quad (\text{E2}) \end{aligned}$$

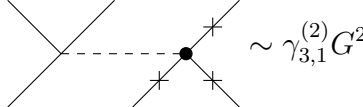
where t_{mn} is a tunneling rate; $\mathcal{K}_n, \mathcal{K}_{mn}, \tilde{\mathcal{K}}_{mn}$ are inter-site spatial overlap integrals; h.c. denotes a Hermitian conjugate, i.e. $(X + \text{h.c.}) \equiv (X + X^\dagger)$; and $\langle i, j \rangle$ denotes the set of all lattice sites i together with their adjacent sites j . Note that we have neglected terms in (E2) which involve more than two field operators addressing states with motional excitations, as these terms will not appear in the leading-order corrections to the effective on-site interaction Hamiltonians. We also still neglect terms which involve products of atomic wavefunctions for motional ground states in different lattice sites.

Diagrammatically representing matrix elements of H_0 and H_{int} which are off-diagonal in lattice site by a dot (i.e. \bullet) and marking lines which represent field operators addressing neighboring lattice sites by a cross (i.e. $+$ or \times , depending on the line orientation), the

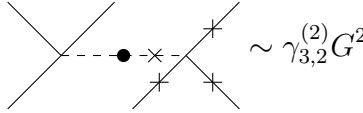
dominant terms in the effective theory which we previously neglected by assuming on-site locality are



$$\sim \gamma_2^{(2)} G^2, \quad \gamma_2^{(2)} \equiv \sum_{n+m>0} \frac{K_{mn} \mathcal{K}_{mn}}{E_{mn}}, \quad (\text{E3})$$



$$\sim \gamma_{3,1}^{(2)} G^2, \quad \gamma_{3,1}^{(2)} \equiv \sum_{n>0} \frac{K_n \mathcal{K}_n}{E_n}, \quad (\text{E4})$$



$$\sim \gamma_{3,2}^{(2)} G^2, \quad \gamma_{3,2}^{(2)} \equiv \sum_{n,m>0} \frac{K_m t_{mn} K_n}{E_m E_n}, \quad (\text{E5})$$

where we have identified, up to an assignment of coupling constants G , the magnitude of all nonzero matrix elements of the diagrams with respect to an eigenbasis of the on-site single-particle Hamiltonian H_0 in (1).

The terms in (E3)-(E5) can be used to estimate an upper bound on the magnitude of dominant corrections to the spectrum of the low-energy theory from off-diagonal (i.e. in lattice site) matrix elements of the Hamiltonians in (E1) and (E2). Conservatively assuming no energetic penalty and no Pauli blocking for any inter-site process, the dominant correction δE_N to the interaction energy of a lattice site with N atoms and b neighboring sites (e.g. $b = 6$ in a primitive cubic lattice) is roughly bounded as

$$|\delta E_N| \lesssim b \binom{N}{2} \max \left\{ \left| \gamma_2^{(2)} \right|, (N-1) \left| \gamma_{3,1}^{(2)} + \gamma_{3,2}^{(2)} \right| \right\} G^2, \quad (\text{E6})$$

where the factor of b accounts for the multiplicity of neighboring sites; the factor of $\binom{N}{2}$ accounts for the number of on-site pairs of atoms which are addressed by the diagrams in (E3)-(E5); and the factor of $N-1$ on $\gamma_{3,X}^{(2)}$ accounts for the number of atoms in a neighboring site which are addressed by the corresponding processes. These factors count the number of matrix elements in the Hamiltonian with magnitude $\sim \gamma_X^{(2)} G^2$. The maximization in (E6) is performed because the relevant two- and three-body processes are mutually exclusive, requiring a different number of atoms on neighboring lattice sites. For a conservative bound of $|\delta E_N|$, the coupling factor G^2 in (E6) can simply be maximized over its allowed values for a given state of atoms on a lattice site, e.g. G_g^2 for a state with no orbital excitations, or $\max \{G_g^2, G_+^2, G_-^2\}$ for a state with one net orbital excitation (in both cases, assuming no orbital excitations in neighboring sites). In the latter case, the bound in (E6) can also be

reduced by observing that to conserve energy, it must be the excited atom which moves to a neighboring site, which reduces the factor of $\binom{N}{2}$ in down to $N - 1$. We emphasize that the bound in (E6) is by no means an exact measure of error, and is merely intended to provide a conservative range of energies and corresponding time scales for which inter-site effects could become relevant despite negligible single-particle ground-state tunneling rates.

Appendix F: Perturbative parameters for the effective theory

The perturbative effective theory developed in Section III is organized in powers of the coupling constants G_X . The formally small, dimensionless quantities for this perturbation theory are the two-body interaction energies KG_X divided by the spectral gap Δ of the non-interacting Hamiltonian H_0 . Here K is a ground-state two-body overlap integral and G_X is a coupling constant. The quantities K , G_X , and Δ all depend on the lattice depth \mathcal{U} . Figure F.1 shows these parameters for the case of ^{87}Sr atoms with $X \in \{\text{gg}, \text{eg}_-, \text{eg}_+, \text{ee}\}$ at lattice depths $\mathcal{U} \in [30, 80] E_R$, where $E_R \approx 3.5 \times 2\pi$ kHz is the lattice photon recoil energy of the atoms. The fact that these perturbative parameters grow with increasing lattice depth \mathcal{U} is a consequence of the fact that the overlap integral K grows faster with \mathcal{U} than the spectral gap Δ . In the case of a harmonic trap with angular frequency ω , for example, by dimensional analysis these parameters would be

$$\frac{K_{\text{HO}}G_X}{\omega} = \frac{G_X}{\omega} \int d^3x |\phi_{\text{HO}}|^4 = \frac{G_X}{\omega} \left[\int dx \left| \left(\frac{m_A \omega}{\pi} \right)^{1/4} e^{-m_A \omega x^2/2} \right|^4 \right]^3 \propto \sqrt{\omega}, \quad (\text{F1})$$

where we assumed that the coupling constants G_X vary weakly with ω . While this result may seem to suggest that the low-energy effective theory should become better at smaller lattice depths, smaller lattice depths also result in increased theoretical uncertainties from the growing relevance of the inter-site effects discussed in Appendix E.

Appendix G: Low-excitation M -body Hamiltonian coefficients

When restricted to the subspace of at most one orbital excitation per lattice site, the M -body Hamiltonians of the low-energy effective theory developed in Section III can be

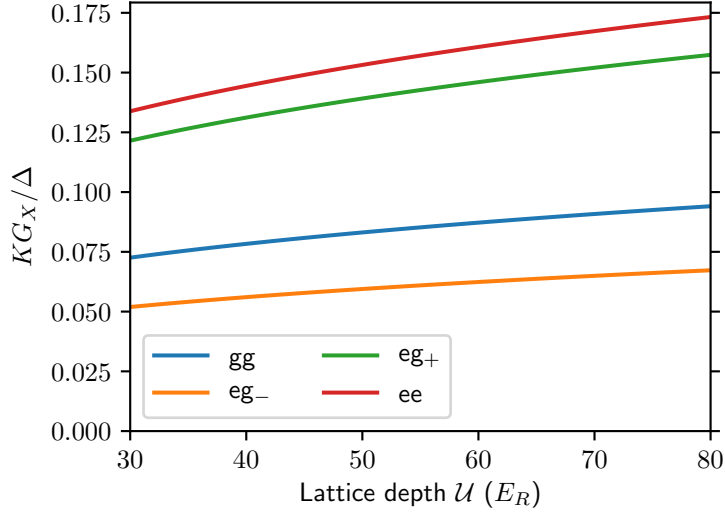


FIG. F.1. Dependence of the perturbative parameters KG_X/Δ on the lattice depth U .

written in the form

$$H_M = \sum_{|\{\mu_j\}|=M} (U_{M,g} \hat{n}_{\mu_1,g} \hat{n}_{\mu_2,g} + U_{M,+} \hat{n}_{\mu_1,e} \hat{n}_{\mu_2,g} + U_{M,-} \hat{c}_{\mu_1,g}^\dagger \hat{c}_{\mu_2,e}^\dagger \hat{c}_{\mu_2,g} \hat{c}_{\mu_1,e}) \prod_{\alpha=3}^M \hat{n}_{\mu_\alpha,g}, \quad (\text{G1})$$

where the coefficients can be expanded as $U_{MX} = \sum_p U_{MX}^{(p)}$ with terms $U_{MX}^{(p)}$ at order p in the coupling constants G_Y . The terms $U_{MX}^{(p)}$ can be determined from the M -body p -order Hamiltonians $H_M^{(p)}$ derived in section III, i.e. in (17), (19), (36), and (46). For the effective 2-, 3-, and 4-body Hamiltonians through third order in the coupling constants, the coefficients are

$$U_{2,g} = \frac{1}{2} \alpha_2^{(1)} G_g, \quad U_{2,+} = \alpha_2^{(1)} G_+, \quad U_{2,-} = \alpha_2^{(1)} G_-, \quad (\text{G2})$$

$$U_{3,g}^{(2)} = -\alpha_3^{(2)} G_g^2, \quad U_{3,+}^{(2)} = -\alpha_3^{(2)} G_+ (G_+ + 2G_g), \quad (\text{G3})$$

$$U_{3,-}^{(2)} = -\alpha_3^{(2)} G_- (2G_+ + G_- + 2G_g), \quad (\text{G4})$$

$$U_{3,g}^{(3)} = (\alpha_{3,1}^{(3)} - \alpha_5^{(3)}) 2G_g^3 + (2\alpha_{3,2}^{(3)} - \alpha_{4,3}^{(3)} - \alpha_5^{(3)}) G_g^3, \quad (\text{G5})$$

$$U_{3,+}^{(3)} = (\alpha_{3,1}^{(3)} - \alpha_5^{(3)}) (G_+^3 + 4G_+^2 G_g + G_+ G_-^2 + G_+ G_g^2 + G_-^3 + G_-^2 G_g) + (2\alpha_{3,2}^{(3)} - \alpha_{4,3}^{(3)} - \alpha_5^{(3)}) (G_+^3 + G_+^2 G_g + G_+ G_-^2 + G_+ G_g^2 + G_-^2 G_g), \quad (\text{G6})$$

$$U_{3,-}^{(3)} = \left(\alpha_{3,1}^{(3)} - \alpha_5^{(3)} \right) G_- \left(3G_+^2 + 2G_+G_- + 8G_+G_g + 3G_-G_g + G_g^2 \right) + \left(2\alpha_{3,2}^{(3)} - \alpha_{4,3}^{(3)} - \alpha_5^{(3)} \right) G_- \left(3G_+^2 + 2G_+G_- + 2G_+G_g + G_-^2 + G_g^2 \right), \quad (\text{G7})$$

$$U_{4,g}^{(3)} = \left(2\alpha_{4,1}^{(3)} - \alpha_5^{(3)} \right) G_g^3 + \left(\alpha_{4,2}^{(3)} - \alpha_5^{(3)} \right) 2G_g^3, \quad (\text{G8})$$

$$U_{4,+}^{(3)} = \left(2\alpha_{4,1}^{(3)} - \alpha_5^{(3)} \right) 2G_+G_g \left(G_+ + G_g \right) + \left(\alpha_{4,2}^{(3)} - \alpha_5^{(3)} \right) G_+ \left(G_+^2 + 2G_+G_g + 5G_g^2 \right), \quad (\text{G9})$$

$$U_{4,-}^{(3)} = \left(2\alpha_{4,1}^{(3)} - \alpha_5^{(3)} \right) 2G_-G_g \left(2G_+ + G_- + G_g \right) + \left(\alpha_{4,2}^{(3)} - \alpha_5^{(3)} \right) G_- \left(3G_+^2 + 3G_+G_- + 4G_+G_g + G_-^2 + 2G_-G_g + 5G_g^2 \right), \quad (\text{G10})$$

In terms of the spatial overlap integrals defined in (6) and (8), the prefactors $\alpha_X^{(p)}$ on the coefficients $U_X^{(p)}$ are

$$\alpha_2^{(1)} \equiv K, \quad \alpha_3^{(2)} \equiv \sum_{n>0} \frac{K_n^2}{E_n}, \quad \alpha_5^{(3)} \equiv K \sum_{n>0} \frac{K_n^2}{E_n^2}, \quad (\text{G11})$$

$$\alpha_{3,1}^{(3)} \equiv \sum_{\substack{\ell+m>0 \\ \ell+n>0}} \frac{K_{\ell m} K_n^m K_{\ell n}}{E_{\ell m} E_{\ell n}}, \quad \alpha_{3,2}^{(3)} \equiv \sum_{\substack{\ell+m>0 \\ n>0}} \frac{K_{\ell m} K_n}{E_{\ell m} E_n} \left(K_n^{\ell m} - \frac{K_{\ell m} K_n}{K} \right), \quad (\text{G12})$$

$$\alpha_{4,1}^{(3)} \equiv \sum_{\substack{m>0 \\ n>0}} \frac{K_{mn} K_m K_n}{E_{mn} E_n}, \quad \alpha_{4,2}^{(3)} \equiv \sum_{m,n>0} \frac{K_m K_n^m K_n}{E_m E_n}, \quad \alpha_{4,3}^{(3)} \equiv K \sum_{m+n>0} \frac{K_{mn}^2}{E_{mn}^2}. \quad (\text{G13})$$

-
- [1] A. Derevianko and H. Katori, [Reviews of Modern Physics](#) **83**, 331 (2011).
- [2] H. Katori, [Nature Photonics](#) **5**, 203 (2011).
- [3] A. D. Ludlow, M. M. Boyd, J. Ye, E. Peik, and P. O. Schmidt, [Reviews of Modern Physics](#) **87**, 637 (2015).
- [4] S. G. Porsev and A. Derevianko, [Physical Review A](#) **69**, 042506 (2004).
- [5] R. Santra, K. V. Christ, and C. H. Greene, [Physical Review A](#) **69**, 042510 (2004).
- [6] B. J. Bloom, T. L. Nicholson, J. R. Williams, S. L. Campbell, M. Bishof, X. Zhang, W. Zhang, S. L. Bromley, and J. Ye, [Nature](#) **506**, 71 (2014).

- [7] T. L. Nicholson, S. L. Campbell, R. B. Hutson, G. E. Marti, B. J. Bloom, R. L. McNally, W. Zhang, M. D. Barrett, M. S. Safronova, G. F. Strouse, W. L. Tew, and J. Ye, [Nature Communications](#) **6**, 6896 (2015).
- [8] S. L. Campbell, R. B. Hutson, G. E. Marti, A. Goban, N. D. Oppong, R. L. McNally, L. Sonderhouse, J. M. Robinson, W. Zhang, B. J. Bloom, and J. Ye, [Science](#) **358**, 90 (2017).
- [9] A. J. Daley, M. M. Boyd, J. Ye, and P. Zoller, [Physical Review Letters](#) **101**, 170504 (2008).
- [10] A. V. Gorshkov, A. M. Rey, A. J. Daley, M. M. Boyd, J. Ye, P. Zoller, and M. D. Lukin, [Physical Review Letters](#) **102**, 110503 (2009).
- [11] A. J. Daley, [Quantum Information Processing](#) **10**, 865 (2011), [arXiv:1106.5712](#).
- [12] A. J. Daley, J. Ye, and P. Zoller, [The European Physical Journal D](#) **65**, 207 (2011).
- [13] M. D. Swallows, M. Bishof, Y. Lin, S. Blatt, M. J. Martin, A. M. Rey, and J. Ye, [Science](#) **331**, 1043 (2011).
- [14] N. D. Lemke, J. vonStecher, J. A. Sherman, A. M. Rey, C. W. Oates, and A. D. Ludlow, [Physical Review Letters](#) **107**, 103902 (2011).
- [15] S. Taie, R. Yamazaki, S. Sugawa, and Y. Takahashi, [Nature Physics](#) **8**, 825 (2012).
- [16] M. J. Martin, M. Bishof, M. D. Swallows, X. Zhang, C. Benko, J. von-Stecher, A. V. Gorshkov, A. M. Rey, and J. Ye, [Science](#) **341**, 632 (2013).
- [17] F. Scazza, C. Hofrichter, M. Hfer, P. C. D. Groot, I. Bloch, and S. Flling, [Nature Physics](#) **10**, 779 (2014).
- [18] G. Cappellini, M. Mancini, G. Pagano, P. Lombardi, L. Livi, M. Siciliani de Cumis, P. Cancio, M. Pizzocaro, D. Calonico, F. Levi, C. Sias, J. Catani, M. Inguscio, and L. Fallani, [Physical Review Letters](#) **113**, 120402 (2014).
- [19] X. Zhang, M. Bishof, S. L. Bromley, C. V. Kraus, M. S. Safronova, P. Zoller, A. M. Rey, and J. Ye, [Science](#) **345**, 1467 (2014).
- [20] A. M. Rey, A. V. Gorshkov, C. V. Kraus, M. J. Martin, M. Bishof, M. D. Swallows, X. Zhang, C. Benko, J. Ye, N. D. Lemke, and A. D. Ludlow, [Annals of Physics](#) **340**, 311 (2014).
- [21] M. A. Cazalilla, A. F. Ho, and M. Ueda, [New Journal of Physics](#) **11**, 103033 (2009).
- [22] M. Hermele, V. Gurarie, and A. M. Rey, [Physical Review Letters](#) **103**, 135301 (2009).
- [23] M. Hermele and V. Gurarie, [Physical Review B](#) **84**, 174441 (2011).
- [24] G. Chen, K. R. A. Hazzard, A. M. Rey, and M. Hermele, [Physical Review A](#) **93**, 061601 (2016).

- [25] P. A. Lee, N. Nagaosa, and X.-G. Wen, [Reviews of Modern Physics](#) **78**, 17 (2006).
- [26] P. A. Lee, [Reports on Progress in Physics](#) **71**, 012501 (2008).
- [27] S.-S. Gong, W. Zhu, and D. N. Sheng, [Scientific Reports](#) **4**, 6317 (2014).
- [28] M. Freedman, C. Nayak, K. Shtengel, K. Walker, and Z. Wang, [Annals of Physics](#) **310**, 428 (2004).
- [29] Wiese U.-J., [Annalen der Physik](#) **525**, 777 (2013).
- [30] E. Zohar, J. I. Cirac, and B. Reznik, [Reports on Progress in Physics](#) **79**, 014401 (2016).
- [31] D. Banerjee, M. Bgüli, M. Dalmonte, E. Rico, P. Stebler, U.-J. Wiese, and P. Zoller, [Physical Review Letters](#) **110**, 125303 (2013).
- [32] E. Rico, M. Dalmonte, P. Zoller, D. Banerjee, M. Bögli, P. Stebler, and U. J. Wiese, [Annals of Physics](#) **393**, 466 (2018).
- [33] C. Wu, J.-p. Hu, and S.-c. Zhang, [Physical Review Letters](#) **91**, 186402 (2003).
- [34] A. Goban, R. B. Hutson, G. E. Marti, S. L. Campbell, M. A. Perlin, P. S. Julienne, J. P. D’Incao, A. M. Rey, and J. Ye, [Nature](#) **563**, 369 (2018).
- [35] P. R. Johnson, D. Blume, X. Y. Yin, W. F. Flynn, and E. Tiesinga, [New Journal of Physics](#) **14**, 053037 (2012).
- [36] X. Y. Yin, D. Blume, P. R. Johnson, and E. Tiesinga, [Physical Review A](#) **90**, 043631 (2014).
- [37] P. R. Johnson, E. Tiesinga, J. V. Porto, and C. J. Williams, [New Journal of Physics](#) **11**, 093022 (2009).
- [38] S. Will, T. Best, U. Schneider, L. Hackermüller, D.-S. Lühmann, and I. Bloch, [Nature](#) **465**, 197 (2010).
- [39] M. J. Mark, E. Haller, K. Lauber, J. G. Danzl, A. J. Daley, and H.-C. Nägerl, [Physical Review Letters](#) **107**, 175301 (2011).
- [40] G. E. Marti, R. B. Hutson, A. Goban, S. L. Campbell, N. Poli, and J. Ye, [Physical Review Letters](#) **120**, 103201 (2018).
- [41] J. Ye, H. J. Kimble, and H. Katori, [Science](#) **320**, 1734 (2008).
- [42] A. V. Gorshkov, M. Hermele, V. Gurarie, C. Xu, P. S. Julienne, J. Ye, P. Zoller, E. Demler, M. D. Lukin, and A. M. Rey, [Nature Physics](#) **6**, 289 (2010).
- [43] M. L. Wall and L. D. Carr, [Physical Review A](#) **87**, 033601 (2013).
- [44] T. Busch, B.-G. Englert, K. Rzażewski, and M. Wilkens, [Foundations of Physics](#) **28**, 549 (1998).

- [45] S. Giorgini, L. P. Pitaevskii, and S. Stringari, *Reviews of Modern Physics* **80**, 1215 (2008).
- [46] D. Blume and C. H. Greene, *Physical Review A* **65**, 043613 (2002).
- [47] V. V. Flambaum, G. F. Gribakin, and C. Harabati, *Physical Review A* **59**, 1998 (1999).
- [48] W. Kohn, *Physical Review* **115**, 809 (1959).
- [49] S. Bravyi, D. P. DiVincenzo, and D. Loss, *Annals of Physics* **326**, 2793 (2011).
- [50] J. R. Schrieffer and P. A. Wolff, *Physical Review* **149**, 491 (1966).
- [51] C. Davis and W. M. Kahan, *Bulletin of the American Mathematical Society* **75**, 863 (1969).
- [52] E. Brion, L. H. Pedersen, and K. Mølmer, *Journal of Physics A: Mathematical and Theoretical* **40**, 1033 (2007).
- [53] D. F. James and J. Jerke, *Canadian Journal of Physics* **85**, 625 (2007).
- [54] F. Reiter and A. S. Sørensen, *Physical Review A* **85**, 032111 (2012).
- [55] M. Sanz, E. Solano, and Í. L. Egusquiza, in *Applications + Practical Conceptualization + Mathematics = Fruitful Innovation*, Mathematics for Industry (Springer, Tokyo, 2016) pp. 127–142.
- [56] X.-P. Zang, M. Yang, F. Ozaydin, W. Song, and Z.-L. Cao, *Scientific Reports* **5**, 16245 (2015).
- [57] H. P. Büchler, *Physical Review Letters* **104**, 090402 (2010).
- [58] D. B. M. Dickerscheid, U. Al Khawaja, D. van Oosten, and H. T. C. Stoof, *Physical Review A* **71**, 043604 (2005).